Biochemical Pharmacology 203 (2022) 115202

Contents lists available at ScienceDirect

Biochemical Pharmacology

journal homepage: www.elsevier.com/locate/biochempharm

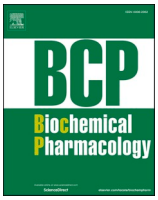

Review

Rotational constriction of curcuminoids impacts 5-lipoxygenase and mPGES-1 inhibition and evokes a lipid mediator class switch in macrophages

Zhigang Rao [a,1], Diego Caprioglio [b,1], André Gollowitzer [a], Christian Kretzer [c], Daniela Imperio [b], Juan A. Collado [d,e,f], Lorenz Waltl [a], Sandra Lackner [a], Giovanni Appendino [b], Eduardo Muñoz [d,e,f], Veronika Temml [g], Oliver Werz [c], Alberto Minassi [b,*], Andreas Koeberle [a,*]

[a] Michael Popp Institute and Center for Molecular Biosciences Innsbruck (CMBI), University of Innsbruck, Innsbruck 6020, Austria
[b] Department of Drug Science, University of Piemonte Orientale, 28100 Novara, Italy
[c] Department of Pharmaceutical/Medicinal Chemistry, Institute of Pharmacy, Friedrich Schiller University Jena, Jena 07743, Germany
[d] Department of Cellular Biology, Physiology and Immunology, University of Cordoba, 14071, Cordoba, Spain
[e] Instituto Maimónides de Investigación Biomédica de Córdoba (IMIBIC), 14004, Cordoba, Spain
[f] Hospital Universitario Reina Sofia, 14004, Cordoba, Spain
[g] Institute of Pharmacy, Department of Pharmaceutical and Medicinal Chemistry, Paracelsus Medical University Salzburg, Salzburg 5020, Austria

ARTICLE INFO

Keywords:
Natural product
Curcumin
Inflammation
Lipid mediators
Leukotriene
Structure–activity relationship

ABSTRACT

Polypharmacological targeting of lipid mediator networks offers potential for efficient and safe anti-inflammatory therapy. Because of the diversity of its biological targets, curcumin (**1a**) has been viewed as a privileged structure for bioactivity or, alternatively, as a pan-assay interference (PAIN) compound. Curcumin has actually few high-affinity targets, the most remarkable ones being 5-lipoxygenase (5-LOX) and microsomal prostaglandin E_2 synthase (mPGES)-1. These enzymes are critical for the production of pro-inflammatory leukotrienes and prostaglandin (PG)E_2, and previous structure–activity-relationship studies in this area have focused on the enolized 1,3-diketone motif, the alkyl-linker and the aryl-moieties, neglecting the rotational state of curcumin, which can adopt twisted conformations in solution and at target sites. To explore how the conformation of curcuminoids impacts 5-LOX and mPGES-1 inhibition, we have synthesized rotationally constrained analogues of the natural product and its pyrazole analogue by alkylation of the linker and/or of the *ortho* aromatic position(s). These modifications strongly impacted 5-LOX and mPGES-1 inhibition and their systematic analysis led to the identification of potent and selective 5-LOX (**3b**, IC_{50} = 0.038 μM, 44.7-fold selectivity over mPGES-1) and mPGES-1 inhibitors (**2f**, IC_{50} = 0.11 μM, 4.6-fold selectivity over 5-LOX). Molecular docking experiments suggest that the *C*2-methylated pyrazolocurcuminoid **3b** targets an allosteric binding site at the interface between catalytic and regulatory 5-LOX domain, while the *o, o*'-dimethylated desmethoxycurcumin **2f** likely binds between two monomers of the trimeric mPGES-1 structure. Both compounds trigger a lipid mediator class switch from pro-inflammatory leukotrienes to PG and specialized pro-resolving lipid mediators in activated human macrophages.

Abbreviations: AA, arachidonic acid; COX, cyclooxygenase; FCS, fetal calf serum; GCC, gravity column chromatography; 5-LOX, 5-lipxoygenase; LTs, leukotrienes; mPGES-1, microsomal prostaglandin E_2 synthase-1; Nrf2, nuclear factor-erythroid 2-related factor-2; NF-κB, nuclear factor κB; PAIN, pan assay interference compound; PBMC, peripheral blood mononuclear cells; PMNL, polymorphonuclear leukocytes; PG, prostaglandin; STAT3, signal transducer and activator of transcription 3; SPM, specialized pro-resolving mediators; SACM, *Staphylococcus aureus*-conditioned medium; SAR, structure–activity relationship; UPLC-MS/MS, ultra-performance liquid chromatography-tandem mass spectrometry.

* Corresponding authors at: Department of Drug Science, University of Piemonte Orientale, Largo Donegani 2/3, Novara 28100, Italy (A. Minassi). Michael Popp Institute and Center for Molecular Biosciences Innsbruck (CMBI), University of Innsbruck, Mitterweg 24, 6020 Innsbruck, Austria (A. Koeberle).
E-mail addresses: alberto.minassi@uniupo.it (A. Minassi), andreas.koeberle@uibk.ac.at (A. Koeberle).

[1] The authors equally contributed to the study.

https://doi.org/10.1016/j.bcp.2022.115202
Received 18 May 2022; Received in revised form 28 July 2022; Accepted 29 July 2022
Available online 3 August 2022

1. Introduction

5-Lipoxygenase (5-LOX) and microsomal prostaglandin E synthase-1 (mPGES-1) are critically involved in the biosynthesis of pro-inflammatory lipid mediators, i.e., leukotrienes (LTs) and prostaglandin (PG)E_2, and contribute to the initiation and progression of inflammation and tumorigenesis [1,2]. 5-LOX receives arachidonic acid (AA) from 5-LOX-activating protein and generates LTA_4 in a two-step reaction involving C5-peroxidation and subsequent dehydration under formation of a conjugated epoxide [3]. LTA_4 is either converted to LTB_4, a potent chemoattractant, or to cysteinyl-LT, which support edema formation and trigger bronchoconstriction [4]. The inducible isoenzyme mPGES-1 is functionally coupled to cyclooxygenase (COX)-2 and converts PGH_2 into PGE_2, the major prostanoid regulating inflammation [5]. Unlike the flat structure–activity relationship (SAR) of **1a** derivatives on other anti-inflammatory targets (i.e., nuclear factor (NF)-κB and COX), the inhibitory activity of **1a** on 5-LOX and mPGES-1 can be clearly dissected. Aryl-prenylation [6,7], shortening of the alkyl chain [8], or replacement of the enolized dicarbonyl moiety by either pyrazole [9] or triazole [10] are effective means to manipulate the inhibitory potency and target selectivity of curcuminoids towards 5-LOX and mPGES-1.

The orange diarylheptanoid curcumin (monomolecular curcumin, purcumin, **1a**) is considered the major bioactive constituent of turmeric (*Curcuma longa* L.), where it occurs along with related minor analogues, such as desmethoxycurcumin and bisdesmethoxycurcumin (**2a**). Turmeric is used in Ayurvedic and traditional Chinese medicine as remedy against biliary disorders, anorexia, coryza, cough, diabetic wounds, hepatic disorder, rheumatism, and sinusitis [11]. Pre-clinical studies on **1a** have shown anti-oxidative, anti-inflammatory as well as anti-tumoral properties [12], but the clinical translation of this potential is limited by poor bioavailability and metabolic stability [13]. Membrane disruption [14], redox reactivity [15,16], and Michael acceptor behavior [17] underlie the promiscuous bioactivity profile of **1a**, which has been considered an archetypal pan assay interference compound (PAIN). Many **1a** targets are associated to inflammation, as exemplified by the nuclear factor-erythroid 2-related factor-2 (Nrf2) [18], NF-κB [19], COX isoenzymes [20,21], and signal transducer and activator of transcription (STAT)3 [22]. The SARs of **1a** are generally flat [23], with efficacious concentrations in the range of 10–50 μM and largely exceeding the plasma concentrations (as conjugates) observed upon oral administration [24]. Multi-target micromolar activities aside, compound **1a** has few high-affinity targets with IC_{50} values in the sub-micromolar range, the most important being 5-LOX and mPGES-1 [21,25].

Compound **1a** undergoes keto-enol tautomerism, with the enol form

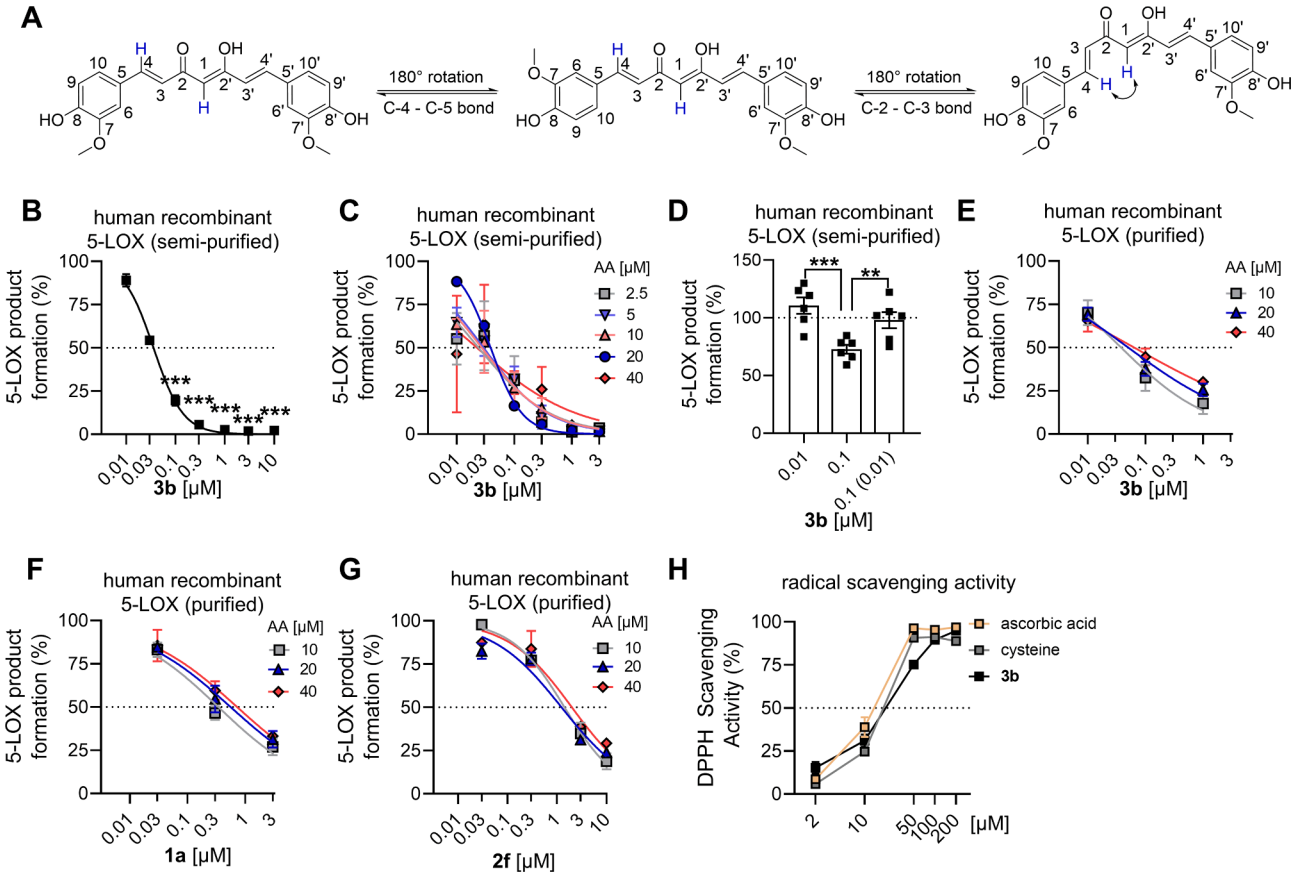

Fig. 1. The curcumin derivative **3b** potently inhibits human recombinant 5-LOX. (A) Rotameric equilibration of curcumin enol tautomers. (B-G) 5-LOX product formation was initiated by arachidonic acid (AA; 20 μM, B, D; 2.5–40 μM, C; 10–40 μM, E-G) and 5-LOX products (et-LTB_4, t-LTB_4 and 5-H(p)ETE) were analyzed by RP-UV-HPLC. (B) Effect of **3b** (0.01–10 μM) on human recombinant 5-LOX. (C, E-G) Dependency of 5-LOX (semi-purified, C; purified, E-G) inhibition by **3b** (0.01–3 μM), **1a** (0.03–3 μM) or **2f** (0.03–10 μM) on the substrate (AA) concentration. (D) Reversibility of 5-LOX inhibition. Human recombinant 5-LOX was pre-incubated with vehicle or **3b** (0.01–0.1 μM) and then 10-fold diluted before AA was added. Numbers in brackets indicate the diluted compound concentration after pre-incubation. (H) Scavenging of 2,2-diphenyl-1-picrylhydrazyl (DPPH) radicals by **3b**, cysteine and ascorbic acid (2–200 μM). Results are given as means ± S.E.M., percentage of vehicle control, n = 3 (B, H), n = 2–3 (C, E-G), n = 6 (D). Absolute values for vehicle control in B): 838 ± 87 pg; C): 185 ± 43 pg, 2.5 μM AA; 316 ± 82 pg, 5 μM AA; 644 ± 218 pg, 10 μM AA; 608 ± 97 pg, 20 μM AA; 423 ± 153 pg, 40 μM AA; D): 959 ± 226 pg; E-G) 2365 ± 116 pg, 10 μM AA; 2467 ± 94 pg, 20 μM AA; 2771 ± 74 pg, 40 μM AA; H) 0.13 ± 0.01 a.u. Data were log-transformed for statistical analysis. ***$p < 0.001$, **$p < 0.01$; repeated measures one-way ANOVA plus Dunnett's (B) or Tukey's (D) *post hoc* test.

being the dominant tautomer, and is generally represented in a linear conformation. However, nuclear magnetic resonance analysis of molecular flexibility in solution showed that **1a** adopts multiple conformations in solution, which includes flat, twisted and partially bend three-dimensional geometries [26]. While flat structures were observed in single-crystal structures [27], twisted conformations of **1a** seem more relevant in the interaction with proteins at specific binding sites, as suggested by docking studies for human mPGES-1 [6], soybean LOX [28] and human platelet 12-LOX [29]. Linear and twisted confirmations of **1a** are interconverted by rotation around the $C2^{(')}$–$C3^{(')}$ sigma bond linking the olefin and the carbonyl functions. Rotation around the $C4^{(')}$-$C5^{(')}$ aryl-vinyl bond also takes place in solution, interconverting conformations with the methoxy on the same side and on opposite site of the enolic (carbonyl) oxygen (Fig. 1**A**). To affect this equilibration and raise their energetic burden, alkyl group(s) were introduced on the *ortho* aryl carbon(s) and on the vinyl carbon adjacent to the carbonyl ($C3^{(')}$). Our SAR studies strongly support the view that inhibition of the high-affinity targets mPGES-1 and 5-LOX by curcuminoids require specific twisted conformations and that the fixation of such is an effective mean to enhance potency and/or selectivity.

2. Materials and methods

2.1. Materials

MK-886, zileuton, deuterated internal standards and non-deuterated lipid mediator standards for ultra-performance liquid chromatography-tandem mass spectrometry (UPLC-MS/MS) were purchased from Cayman Chemical (Ann Arbor, MI). Compound **3a** and **4a** were synthesized as described [9,30]. Compounds **1a** and **2a**, staurosporine, BWA4C, calcium ionophore (A23187) and all other reagents were obtained from Merck (Darmstadt, Germany) unless mentioned otherwise.

2.2. Chemistry

2.2.1. General experimental procedures

IR spectra were recorded on an Avatar 370 FT-IR Techno-Nicolet apparatus. ^{1}H (400 MHz) and ^{13}C (100 MHz) NMR spectra were measured on a Bruker Avance 400 MHz spectrometer. Chemical shifts were referenced to the residual solvent signal ($CDCl_3$: $\delta H = 7.25$, $\delta C = 77.0$, CD_3OD: $\delta H = 3.34$, $\delta C = 49.0$, DMSO: $\delta H = 2.50$, $\delta C = 39.5$, $(CO(CD_3)_2$: $\delta H = 2.05$, $\delta C = 206.7$, 29.9). Low- and high-resolution electrospray ionization mass spectrometry data were determined on an LTQ OrbitrapXL (Thermo Scientific) mass spectrometer. Chemical reactions were monitored by thin-layer chromatography by visualizing educts and products on Merck 60 F254 (0.25 mm) plates upon staining with 5 % H_2SO_4 in EtOH and heating. Organic phases were dried with Na_2SO_4 before evaporation. Chemical reagents and solvents were purchased from Merck, TCI Europe or Fluorochem and were used without additional purification unless stated otherwise. Petroleum ether with boiling point of 40–60 °C was used. Silica gel 60 (70–230 mesh) was used for gravity column chromatography (GCC).

2.2.2. General procedure for the synthesis of constrained curcuminoids

To a stirred solution of an aromatic aldehyde (**5**–**8**) (2 eq. mol) in dry DMF (2 mL/ mmol), a complementary 1,3-diketo derivative (**9**–**13**) (1 eq. mol), B_2O_3 (1.6 eq. mol), $B(OCH_3)_3$ (0.73 eq. mol) and *n*-butyl amine (0.08 eq. mol) were sequentially added. The solution was stirred at 40 °C until substantial conversion was observed by thin-layer chromatography, then quenched with H_2SO_4 (2 M) and extracted with EtOAc. The organic layer was dried over Na_2SO_4, filtered, and evaporated. Compounds **1b-1e** and **2a-2 g**, were obtained after purification by GCC on silica gel. Compounds **2a-2e** were not purified, but the crude material was directly used in the synthesis of the corresponding pyrazoles.

2.2.2.1. (1E,4Z,6E)-5-Hydroxy-1,7-bis(4-hydroxy-3-methoxyphenyl)-2-methylhepta-1,4,6-trien-3-one (1b). ^{1}H NMR (400 MHz, $(CO(CD_3)_2)$ δ: 8.12 (OH, bs, 1H), 8.01 (OH, bs, 1H), 7.59 (t, $J = 7.9$ Hz, 2H), 7.33 (s, 1H), 7.22 – 7.11 (m, 2H), 7.07 (dd, $J_1 = 8.3$ Hz, $J_2 = 1.9$ Hz, 1H), 6.89 (t, $J = 8.4$ Hz,1H), 6.74 (d, $J = 15.8$ Hz,1H), 6.30 (s, 1H), 3.94 (s, 3H), 3.91 (s, 3H), 2.17 (s, 3H); ^{13}C NMR (100 MHz, $CO(CD_3)_2$) δ: 189.95, 180.58, 149.01, 147.93, 147.45, 147.38, 139.79, 136.64, 131.71, 128.07, 127.42, 123.94, 122.86, 121.20, 115.39, 115.13, 113.66, 110.50, 97.10, 55.44, 29.60, 29.41, 29.22, 29.03, 28.83, 28.64, 28.45, 12.90. HRESIMS *m/z* $[M + H]^+$ 383.14878 (calcd for $C_{22}H_{23}O_6$, 383.14891).

2.2.2.2. (1E,4Z,6E)-5-Hydroxy-1,7-bis(4-hydroxy-3-methoxyphenyl)-2,6-dimethylhepta-1,4,6-trien-3-one (1c). ^{1}H NMR (400 MHz, $(CO(CD_3)_2)$ δ: 7.99 (OH, s, 2H), 7.62 (s, 1H), 7.13 (d, $J = 1.7$ Hz, 2H), 7.06 (dd, $J_1 = 8.2$ Hz, $J_2 = 1.6$ Hz, 1H), 6.89 (d, $J = 8.2$ Hz, 1H), 6.57 (s, 1H), 3.89 (s, 6H), 2.19 (s, 6H); ^{13}C NMR (100 MHz, $CO(CD_3)_2$) δ: 196.66, 187.10, 147.33, 147.30, 136.11, 131.18, 128.14, 123.81, 115.04, 113.64, 93.02, 55.43, 55.41, 13.03. HRESIMS *m/z* $[M + H]^+$ 395.16428 (calcd for $C_{23}H_{25}O_6$, 397.16456).

2.2.2.3. (1E,4Z)-5-Hydroxy-6-((E)-4-hydroxy-3-methoxybenzylidene)-1-(4-hydroxy-3-methoxyphenyl)-octa-1,4-dien-3-one (1d). ^{1}H NMR (400 MHz, $(CO(CD_3)_2)$ δ: 8.12 (OH, bs, 1H), 8.03 (OH, bs, 1H), 7.59 (d, $J = 15.8$ Hz, 1H), 7.53 (s, 1H), 7.33 (d, $J = 1.7$ Hz, 1H), 7.16 (dd, $J1 = 8.1$ Hz, $J2 = 1.8$ Hz, 2H), 7.11 (d, $J = 1.7$ Hz, 1H), 7.05 (dd, $J1 = 8.4$ Hz, $J2 = 1.7$ Hz, 2H), 6.89 (dd, $J1 = 10.0$ Hz, $J2 = 8.2$ Hz, 2H), 6.74 (d, $J = 15.8$ Hz, 1H), 6.30 (s, 1H), 3.91 (s,3H), 3.89 (s, 3H), 2.67 (q, $J = 7.5$ Hz, 4H), 1.21 (t, $J = 7.5$ Hz, 3H); ^{13}C NMR (100 MHz, $CO(CD_3)_2$) δ: 190.23, 190.16, 148.90, 147.88, 147.50, 147.43, 136.26, 127.77, 127.45, 123.39, 122.80, 121.09, 121.05, 115.31, 115.22, 113.19, 110.45, 97.21, 55.43, 55.35, 19.69, 13.26. HRESIMS *m/z* $[M + H]^+$ 397.16412 (calcd for $C_{23}H_{25}O_6$, 397.16456).

2.2.2.4. (Z)-6-Hydroxy-3,7-bis((E)-4-hydroxy-3-methoxybenzylidene) non-5-en-4-one (1e). ^{1}H NMR (400 MHz, $(CO(CD_3)_2)$ δ: 7.56 (s, 2H), 7.11 (d, $J = 1.9$ Hz, 2H), 7.04 (dd, $J_1 = 8.1$ Hz, $J_2 = 2.0$ Hz, 2H), 6.91(d, $J = 8.2$ Hz, 2H), 6.58 (s, 1H), 3.89 (s, 6H), 2.69 (q, $J = 7.5$ Hz, 4H), 1.23 (t, $J = 7.5$ Hz, 6H); ^{13}C NMR (100 MHz, $CO(CD_3)_2$) δ: 196.43, 187.05, 147.45, 137.71, 135.67, 127.86, 123.27, 115.20, 113.17, 93.20, 55.35, 19.80, 13.33. HRESIMS *m/z* $[M + H]^+$ 425.19564 (calcd for $C_{25}H_{29}O_6$, 425.19587).

2.2.2.5. (1E,4Z,6E)-5-Hydroxy-1,7-bis(4-hydroxy-2-methylphenyl)hepta-1,4,6-trien-3-one (2f). ^{1}H NMR (400 MHz, $(CO(CD_3)_2)$ δ: 7.90 (d, $J = 15.6$ Hz, 2H), 7.64 (d, $J = 9.2$ Hz, 2H), 6.76 (m, 4H), 6.63 (d, $J = 15.6$ Hz, 2H), 6.01 (s, 1H), 2.41 (s, 6H); ^{13}C NMR (100 MHz, $CO(CD_3)_2$) δ: 183.70, 159.33, 140.01, 137.20, 128.12, 125.37, 121.90, 121.87, 117.38, 113.84, 101.14, 19.00. HRESIMS *m/z* $[M + H]^+$ 337.14313 (calcd for $C_{21}H_{21}O_4$, 337.14344).

2.2.2.6. (1E,4Z,6E)-5-Hydroxy-1,7-bis(4-hydroxy-2,6-dimethylphenyl) hepta-1,4,6-trien-3-one (2 g). ^{1}H NMR (400 MHz, $(CO(CD_3)_2)$ δ: 10.44 (OH, s, 1H), 8.59 (OH, bs, 1H), 7.87 (d, $J = 16.2$ Hz, 2H), 6.64 (s, 4H), 6.38 (d, $J = 16.2$ Hz, 2H), 6.04 (s, 1H), 2.37 (s, 12H); ^{13}C NMR (100 MHz, $CO(CD_3)_2$) δ: 190.70, 157.61, 144.31, 139.40, 138.13, 127.25, 125.42, 116.27, 115.57, 101.20, 20.89. HRESIMS *m/z* $[M + H]^+$ 365.17455 (calcd for $C_{23}H_{25}O_4$, 365.17474).

2.2.3. General procedure for the synthesis of constrained pyrazole-curcuminoids

To a stirred solution of the constrained curcuminoid (1 eq. mol) in acetic acid (2.5 mL/1 mmol), hydrazine monohydrate (2.3 eq. mol) was added. The reaction was stirred at 50 °C overnight, quenched with the addition of brine and extracted with EtOAc. The organic layer was dried over Na_2SO_4, filtered, and evaporated. The residue was purified by GCC

on silica gel.

2.2.3.1. 4-((E)-2-(3-((E)-1-(4-Hydroxy-3-methoxyphenyl)-prop-1-en-2-yl)-1H-pyrazol-5-yl)-vinyl)-2-methoxyphenol (3b). ^{1}H NMR (400 MHz, ($CO(CD_3)_2$) δ: 7.22–6.69 (m, 10*H*), 3.88 (s, 3H), 3.86 (s, 3H) 2.30 (s, 3H); ^{13}C NMR (100 MHz, $CO(CD_3)_2$) δ: 151.04, 147.78, 147.20, 146.85, 146.74, 145.68, 129.95, 129.42, 129.20, 126.37, 126.25, 122.36, 120.24, 115.64, 115.13, 114.84, 112.78, 109.05, 99.01, 55.35, 55.33, 15.27 HRESIMS *m/z* $[M + H]^+$ 379.16530 (calcd for $C_{22}H_{23}N_2O_4$, 379.16523).

2.2.3.2. 4,4′-((1E,1′E)-(1H-Pyrazole-3,5-diyl)bis(prop-1-ene-2,1-diyl))bis (2-methoxyphenol) (3c). ^{1}H NMR (400 MHz, $CO(CD_3)_2$) δ: 7.83 (OH, bs, 2H), 7.00–6.85 (m, 8H), 6.59 (s, 1H), 3.88 (s, 6H), 2.27 (s, 6H); ^{13}C NMR (100 MHz, $CO(CD_3)_2$) δ: 147.19, 145.68, 129.49, 126.33, 126.21, 122.36, 114.83, 112.78, 98.98, 55.38, 15.33. HRESIMS *m/z* $[M + H]^+$ 393.18039 (calcd for $C_{23}H_{25}N_2O_4$, 393.18088).

2.2.3.3. 4-((E)-2-(3-((E)-1-(4-Hydroxy-3-methoxyphenyl)-but-1-en-2-yl)-1H-pyrazol-5-yl)-vinyl)-2-methoxyphenol (3d). ^{1}H NMR (400 MHz, $CO(CD_3)_2$) δ: 7.91–6.70 (m, 10*H*), 3.88 (s, 3H), 3.86 (s, 3H), 2.77 (q, J = 7.4 Hz, 2H), 1.26 (t, J = 7.4 Hz, 3H); ^{13}C NMR (100 MHz, $CO(CD_3)_2$) δ: 149.90, 147.76, 147.26, 146.83, 145.79, 129.87, 129.28, 129.27, 125.96, 121.78, 120.26, 115.71, 115.11, 114.95, 112.30, 109.02, 99.29, 55.36, 55.30, 22.17, 13.56. HRESIMS *m/z* $[M + H]^+$ 393.18051 (calcd for $C_{23}H_{25}N_2O_4$, 393.18088).

2.2.3.4. 4,4′-((1E,1′E)-(1H-Pyrazole-3,5-diyl)bis(but-1-ene-2,1-diyl))bis (2-methoxyphenol) (3e). ^{1}H NMR (400 MHz, ($CO(CD_3)_2$) δ: 6.94–6.70 (m, 8H), 6.51 (s, 1H), 3.84 (s, 6H), 2.71 (q, J = 7.4 Hz, 2H), 1.25 (t, J = 5.8 Hz, 3H); ^{13}C NMR (100 MHz, $CO(CD_3)_2$) δ: 147.27, 145.78, 133.05, 129.34, 125.68, 121.74, 114.97, 112.29, 99.37, 55.30, 22.16, 13.60. HRESIMS *m/z* $[M + H]^+$ 421.21214 (calcd for $C_{25}H_{29}N_2O_4$, 421.21218).

2.2.3.5. 4-((E)-2-(5-((E)-1-(4-Hydroxyphenyl)prop-1-en-2-yl)-1H-pyrazol-3-yl)vinyl)phenol (4b). ^{1}H NMR (400 MHz, $CO(CD_3)_2$) δ: 7.44 (d, J = 8.7 Hz, 2H), 7.30 (d, J = 8.6 Hz, 2H), 7.17 (m, 2H), 7.01 (m, 2H), 6.90 (d, J = 8.6 Hz, 2H), 6.87 (d, J = 8.6 Hz, 2H), 6.73 (s, 1H), 2.31 (s, 3H); ^{13}C NMR (100 MHz, $CO(CD_3)_2$) δ: 157.58, 156.45, 130.60, 129.81, 128.97, 128.68, 127.81, 127.77, 126.24, 115.70, 115.66, 115.23, 99.14, 15.33. HRESIMS *m/z* $[M + H]^+$ 319.14403 (calcd for $C_{20}H_{19}N_2O_2$, 319.14410).

2.2.3.6. 4,4′-((1E,1′E)-(1H-Pyrazole-3,5-diyl)bis(prop-1-ene-2,1-diyl)) diphenol (4c). ^{1}H NMR (400 MHz, $CO(CD_3)_2$) δ: 7.29 (d, J = 8.6 Hz, 4H), 7.10 (brd, 2H), 6.88 (d, J = 8.6 Hz, 4H), 6.73 (s, 1H), 2.99 (s, 6H); ^{13}C NMR (100 MHz, $CO(CD_3)_2$) δ: 156.39, 150.76, 130.53, 128.99, 126.09, 125.95, 115.15, 98.98, 15.26. HRESIMS *m/z* $[M + H]^+$ 333.15937 (calcd for $C_{21}H_{21}N_2O_2$, 333.15975).

2.2.3.7. 4-((E)-2-(5-((E)-1-(4-Hydroxyphenyl)but-1-en-2-yl)-1H-pyrazol-3-yl)vinyl)phenol (4d). ^{1}H NMR (400 MHz, $CO(CD_3)_2$) δ: 7.42 (d, J = 8.6 Hz, 2H), 7.30 (d, J = 8.6 Hz, 2H), 7.15 (d, J = 16.5 Hz, 2H), 7.10 (brs, 1H), 6.97 (d, J = 16.5 Hz, 2H), 6.87 (t, J = 8.5 Hz, 4H), 6.71 (s, 1H), 2.74 (q, J = 7.4 Hz, 4H), 1.22 (t, J = 7.4 Hz, 6H); ^{13}C NMR (100 MHz, $CO(CD_3)_2$) δ: 157.43, 156.30, 130.53, 129.43, 129.08, 128.78, 127.72, 127.67, 126.31, 125.87, 115.59, 115.55, 115.46, 115.11, 98.98, 22.10, 13.75. HRESIMS *m/z* $[M + H]^+$ 333.15945 (calcd for $C_{21}H_{21}N_2O_2$, 333.15975).

2.2.3.8. 4,4′-((1E,1′E)-(1H-Pyrazole-3,5-diyl)bis(but-1-ene-2,1-diyl)) diphenol (4e). ^{1}H NMR (400 MHz, $CO(CD_3)_2$) δ: 7.28 (d, J = 8.6 Hz, 4H), 7.03 (s, 2H), 6.89 (d, J = 8.6 Hz, 4H), 6.71 (s, 1H), 2.78 (q, J = 7.4 Hz, 4H), 1.25 (t, J = 7.4 Hz, 6H); ^{13}C NMR (100 MHz, $CO(CD_3)_2$) δ: 156.46, 149.62, 132.83, 130.05, 128.90, 125.51, 115.27, 99.44, 22.06, 13.61. HRESIMS *m/z* $[M + H]^+$ 361.19074 (calcd for $C_{23}H_{25}N_2O_2$, 361.19105).

2.2.3.9. 4,4′-((1E,1′E)-(1H-Pyrazole-3,5-diyl)bis(ethene-2,1-diyl))bis(3-methylphenol) (4f). ^{1}H NMR (400 MHz, $CO(CD_3)_2$) δ: 7.52 (d, J = 1.2 Hz, 2H), 7.39 (d, J = 16.4 Hz, 2H), 6.90 (d, J = 16.4 Hz, 2H), 6.74 (d, J = 3.0 Hz, 2H), 6.71 (s, 3H), 2.36 (s, 6H); ^{13}C NMR (100 MHz, $CO(CD_3)_2$) δ: 157.23, 137.29, 127.45, 127.00, 126.34, 117.02, 116.80, 113.45, 19.13. HRESIMS *m/z* $[M + H]^+$ 333.15946 (calcd for $C_{21}H_{21}N_2O_2$, 333.15975).

2.2.3.10. 4,4′-((1E,1′E)-(1H-Pyrazole-3,5-diyl)bis(ethene-2,1-diyl))bis (3,5-dimethylphenol) (4 g). ^{1}H NMR (400 MHz, $CO(CD_3)_2$) δ: 7.21 (d, J = 16.8 Hz, 2H), 6.76 (s, 1H), 6.60 (s, 4H), 6.58 (d, J = 16.8 Hz, 2H), 2.33 (s, 12H); ^{13}C NMR (100 MHz, $CO(CD_3)_2$) δ: 155.97, 137.50, 127.64, 127.49, 122.87, 115.74, 114.92, 98.95, 20.61. HRESIMS *m/z* $[M + H]^+$ 361.19059 (calcd for $C_{23}H_{25}N_2O_2$, 361.19105).

2.3. Determination of human recombinant 5-LOX activity

The activity of human recombinant 5-LOX was determined as previously described [31]. In brief, *Escherichia coli* Bl21 (DE3) was transformed with pT3–5LO plasmid to express human 5-LOX enzyme. The bacteria were lysed in lysis buffer containing triethanolamine (50 mM), EDTA (5 mM), soybean trypsin inhibitor (60 μg/mL), phenylmethanesulphonyl fluoride (1 mM), dithiothreitol (1 mM) and lysozyme (1 mg/mL). Lysates were collected and sonicated (3 times, 15 s, each) and subjected to differential centrifugation (first 10,000 × g, 15 min; then 40,000 × g, 70 min; at 4 °C). The supernatant was loaded on an ATP-agarose column (Merck) and washed stepwise with a) PBS pH 7.4 plus EDTA (1 mM); b) phosphate buffer (50 mM) containing NaCl (0.5 M) and EDTA (1 mM); and c) phosphate buffer (50 mM) plus EDTA (1 mM). Semi-purified 5-LOX enzyme was eluted with phosphate buffer (50 mM) containing EDTA (1 mM) and ATP (20 mM). Alternatively, human recombinant 5-LOX (formulation: 100 mM Tris-HCl, pH 8.0, containing 5 mM EDTA, 1 mM $CaCl_2$, and 30 % glycerol) was purchased from Cayman Chemical (Batch No. 0633114; Item No. 60402).

To determine 5-LOX activity, semi-purified 5-LOX (0.5 μg) was pretreated with vehicle (DMSO), test compounds or the selective 5-LOX inhibitor BWA4C (0.1 μM, Merck) in 1 mL PBS pH 7.4 plus EDTA (1 mM) and ATP (1 mM) for 10 min at 4 °C. The mixture was pre-warmed for 30 s at 37 °C before 5-LOX product formation was initiated by the addition of AA (20 μM or as indicated, Cayman Chemical) and $CaCl_2$ (2 mM). After 10 min incubation at 37 °C, the reaction was stopped with an equal volume of ice-cold methanol containing the internal standard PGB_1 (2 ng, Cayman Chemical). Lipid mediators formed were extracted by solid phase extraction using Sep-Pak C18 35 cc Vac Cartridges (Waters, Milford, MA). Major 5-LOX products (all-*trans* isomers of LTB_4 and 5-H(p)ETE) were analyzed by RP-UV-HPLC using a Nova-Pak C18 Radial-Pak Column (4 μm, 5 × 100 mm, Waters) under isocratic conditions (73 % methanol/27 % water/0.007 % trifluoroacetic acid) at a flow rate of 1.2 mL/min and detected at 235 nm (for 5-H(p)ETE) or 280 nm (all-*trans* isomers of LTB_4). The 5-LOX reference inhibitor BWA4C (0.1 μM, Merck) inhibited 5-LOX product formation by 87.6 ± 1.7 %.

For the AA competition studies shown in Fig. 1**E-G**, human recombinant 5-LOX (Cayman Chemical, 25–50 units in 1 mL PBS pH 7.4 with 1 mM EDTA and 1 mM ATP) was pre-incubated with vehicle (DMSO), compound **1a**, **3b,** or **2f** for 10 min on ice. Product formation was initiated by the addition of AA (10 μM, 20 μM or 40 μM, Cayman Chemical) and $CaCl_2$ (2 mM) followed by incubation at 37 °C. After 10 min, the reaction was stopped by the addition of ice-cold methanol (1 mL) containing PGB_1 (2 ng, Cayman Chemical) as internal standard. PBS pH 7.4 (498.2 μL) acidified with HCl (1 M, 31.8 μL) was added to the samples, which were centrifuged (750 × g, 10 min, 4 °C) and subjected to solid phase extraction. Clean-Up C-18 Endcapped SPE cartridges (100 mg, 10 mL, UCT, Bristol, PA) were washed twice with methanol and preconditioned with water (1 mL each). Supernatants were loaded onto the

cartridges, which were washed with 1 mL water and 1 mL water/methanol (75/25, v/v) prior to elution of 5-LOX products with 300 μL methanol. After addition of 120 μL water, samples were centrifuged (21,000xg, 10 min, 4 °C) and supernatants subjected to UPLC-photodiode array detector (PDA) analysis.

Chromatographic separation of 5-LOX products (all-*trans* isomers of LTB_4 and 5-H(p)ETE) was performed at 40 °C on a Kinetex C-18 LC column (100 Å, 1.3 μm, 2.1 × 50 mm, Phenomenex, Torrance, CA) using a Nexera X2 UHPLC system (Shimadzu, Kyoto, Japan) that was coupled to a PDA (SPD-M20A, Shimadzu). The UHPLC system was operated at a flow rate of 0.45 mL/min using buffer A (50 % methanol/50 % water/0.05 % trifluoroacetic acid) and buffer B (100 % methanol/0.05 % trifluoroacetic acid). Following sample injection (10 μL), the initial mobile phase composition (A/B = 86/14) was kept constant for 2 min before it was stepwise decreased to A/B = 54/46 (2 min) and then to A/B = 10/90 (another 2 min).

For 5-H(p)ETE analysis, the wavelength was set to 235 nm, whereas PGB_1 (internal standard, Cayman Chemical) and the all-*trans* isomers of LTB_4 were detected at 280 nm. Chromatograms were acquired and processed using LabSolutions (version 5.97, Shimadzu).

2.4. Determination of mPGES-1 activity

mPGES-1 activity was measured in microsomal membranes of IL-1β-treated human lung adenocarcinoma epithelial A549 cells as previously described [32]. Briefly, A549 cells were incubated with IL-1β (2 ng/mL, Peprotech, Hamburg, Germany) in DMEM/high glucose (4.5 g/L) medium plus FCS (10 %) and penicillin/streptomycin (100 U/mL and 100 μg/mL; GE Healthcare, Freiburg, Germany) at 37 °C and 5 % CO_2 for 48 h. Cell pellets were harvested and snap-frozen in liquid nitrogen. After resuspension and incubation in ice-cold homogenization buffer [potassium phosphate buffer (0.1 M, pH 7.4), phenylmethylsulphonyl fluoride (1 mM, Cayman Chemical), soybean trypsin inhibitor (60 μg/mL, Cayman Chemical), leupeptin (1 μg/mL, Cayman Chemical), glutathione (2.5 mM, Cayman Chemical) and sucrose (250 mM, Cayman Chemical)] for 15 min on ice, cells were sonicated (3 times, 20 s, each, at 4 °C). Differential centrifugation (first 10,000 × g, 10 min; then 174,000 × g, 60 min; at 4 °C) yielded the microsomal membrane fraction, which was resuspended in homogenization buffer and diluted in potassium phosphate buffer (0.1 M, pH 7.4) plus glutathione (2.5 mM, Cayman Chemical).

To determine mPGES-1 activity, membranes (containing 2.5–5 μg total protein in 50 μL homogenization buffer) were pre-treated with vehicle (DMSO), test compounds or the mPGES-1 inhibitor MK-886 (10 μM, Cayman Chemical) for 15 min at 4 °C. The formation of PGE_2 was initiated by the addition of PGH_2 [20 μM in 50 μL potassium phosphate buffer (0.1 M, pH 7.4) containing phenylmethylsulphonyl fluoride (1 mM, Cayman Chemical), soybean trypsin inhibitor (60 μg/mL, Cayman Chemical), leupeptin (1 μg/mL, Cayman Chemical), glutathione (2.5 mM, Cayman Chemical)]. After 1 min incubation at 4 °C, the reaction was terminated with an equal volume of stop solution containing $FeCl_2$ (40 mM) and citric acid (80 mM) as well as the internal standard 11β-PGE_2 (1 nmol, Cayman Chemical). The mPGES-1 product PGE_2 was extracted by solid phase extraction using Sep-Pak C18 35 cc Vac Cartridges (Waters), separated on Nova-Pak C18 Radial-Pak Column (4 μm, 5 × 100 mm, Waters) under isocratic conditions (30 % acetonitrile, 70 % water, 0.007 % trifluoroacetic acid) at a flow rate of 1 mL/min and detected at 195 nm. The mPGES-1 reference inhibitor MK-886 (10 μM, Cayman Chemical) inhibited PGE_2 formation by 86.4 ± 0.5 %.

2.5. Molecular docking

Docking simulations were carried out with GOLD (CCDC, version 5.8, Cambridge, UK).

For stable 5-LOX, the compounds were docked in the crystal structure with pdb entry 6NCF, which shows 5-LOX in complex with the allosteric modulator 3-*O*-acetyl-11-keto-β-boswellic acid (AKBA). The binding site was defined in a 12 Å radius around the coordinates 12.86, –22.259, −18.586, and ChemPLP (https://www.ccdc.cam.ac.uk/support-and-resources/support/case/?caseid = 5d1a2fc0-c93a-49c3-a8e2-f95c472dcff0) was used as a scoring function.

The docking simulation on mPGES-1 was conducted on the pdb entry 6VL4 with the co-crystallized ligand DG-035 [33]. The monomeric structure was displayed as a trimer by creating symmetry mates in PyMOL (PyMOL Molecular Graphics System, Version 2.0 Schrödinger, LLC). Water molecules in the binding pocket were set to toggle and spin. The binding site was defined between two monomers in a 12 Å radius around the coordinates 6.321, −14.926, 30.364 (carbon3783 of the co-crystallized ligand). ChemPLP was used as a scoring function. With these settings a redocking was performed and yielded an RMSD of 0.756 Å compared to the crystal structure conformation.

2.6. Isolation of primary immune cells from human blood

Human leukocyte concentrates from whole blood were provided by the Institute for Transfusion Medicine of the University Hospital Jena (Germany). Human peripheral blood mononuclear cells (PBMC) and polymorphonuclear leukocytes (PMNL) were freshly isolated from leukocyte concentrates using a standardized protocol as described [31]. Briefly, leukocytes were first concentrated by dextran sedimentation and then centrifuged on lymphocyte separation medium (LSM 1077, GE Healthcare). After density gradient centrifugation, PBMC and PMNL were collected from the intermediate or bottom layer, respectively. To obtain human monocytes, PBMC were cultured in flasks (Greiner Bio-one, Frickenhausen, Germany) in monocyte medium containing RPMI 1640 with 5 % heat-inactivated fetal calf serum (FCS), L-glutamine (2 mM), and penicillin/streptomycin (100 U/mL and 100 μg/mL; GE Healthcare) for 1.5 h at 37 °C and 5 % CO_2. The adherent monocytes were recovered and their purity was determined as > 85 % by flow cytometric analysis [34]. For further purification of PMNL, erythrocyte contaminants were removed by hypotonic lysis in water. Experiments on human blood and blood cells were approved by the ethical commission of the University Hospital Jena.

2.7. Determination of cellular 5-LOX activity in PMNL

Freshly isolated human PMNL (6×10^6 cells/mL) were resuspended in PBS pH 7.4 with glucose (1 mg/mL) and $CaCl_2$ (1 mM). Cells were first pre-treated with vehicle (DMSO), test compounds or zileuton (3 μM, Cayman Chemical) for 10 min and then co-incubated with AA (20 μM) and calcium ionophore (A23187, 2.5 μM, Merck) for another 10 min at 37 °C. The reaction was terminated with an equal volume of ice-cold methanol containing the internal standard PGB_1 (2 ng, Cayman Chemical). Formed lipid mediators were extracted by solid phase extraction using Sep-Pak C18 35 cc Vac Cartridges (Waters), and major 5-LOX products (LTB_4, its all-trans isomers and 5-H(p)ETE) were analyzed by RP-UV-HPLC as described for the determination of cell-free 5-LOX activity. The 5-LOX reference inhibitor zileuton (3 μM, Cayman Chemical) suppressed 5-LOX product formation by 50.0 ± 20.5 %.

2.8. Differentiation of monocytes to macrophages and polarization into M1 and M2 subtypes

To obtain human monocyte-derived macrophages, freshly isolated human monocytes were stimulated with GM-CSF or M-CSF (20 ng/mL each; Peprotech) for 6–7 days in macrophage medium [RPMI 1640 with 10 % FCS supplemented with L-glutamine (2 mM), penicillin/streptomycin (100 U/mL and 100 μg/mL; GE Healthcare)] at 37 °C and 5 % CO_2. Further polarization of these macrophages for 48 h in macrophage medium with either lipopolysaccharide (LPS, 100 ng/mL) and interferon (IFN)-γ (20 ng/mL, Peprotech) or with interleukin (IL)-4 (20 ng/mL, Peprotech) yielded M1 or M2 phenotypes, respectively [35].

2.9. Treatment of M1 and M2 macrophages and metabololipidomics analysis

Human M1 or M2 macrophages were treated with vehicle (0.1 % DMSO), compound **3b** or **2f** in PBS pH 7.4 plus $CaCl_2$ (1 mM) for 15 min and then stimulated with *Staphylococcus aureus*-conditioned medium (SACM, 1 %) for 180 min at 37 °C. SACM was prepared as previously described [36]. In brief, *Staphylococcus aureus* (strain 6850) was grown for 18 h with orbital shaking (150 rpm) at 37 °C in brain heart infusion medium (Carl Roth, Karlsruhe, Germany). The conditioned medium was harvested after centrifugation (3350 × *g*, 10 min) and sterile filtered using a Millex-GP Syringe Filter Unit (0.22 μm; Merck).

Cell supernatants (1 mL) were collected and mixed with ice-cold methanol (2 mL). d_8-5S-HETE, d_4-LTB_4, d_5-LXA_4, d_5-RvD2, d_4-PGE_2 (200 nM, 10 μL each) and d_8-AA (10 μM, 10 μL) were added as internal standards. Lipid mediators were extracted by solid phase extraction using Sep-Pak C18 6 cc Vac Cartridges (500 mg; Waters), as previously described [37]. Briefly, samples were stored at −20 °C for at least 45 min to allow protein precipitation. After centrifugation (1200 × *g*, 4 °C, 10 min), the supernatant was combined with acidified water (pH 3.5, 7 mL) and loaded onto pre-equilibrated solid phase cartridge columns. Washing steps with water and *n*-hexane (6 mL, each) followed. Lipid mediators were eluted with methyl formate (6 mL), brought to dryness using an evaporation system (TurboVap LV, Biotage, Uppsala, Sweden) and resuspended in methanol/water (50/50, v/v, 100 μL) for UPLC-MS/MS analysis.

For metabololipidomics analysis, lipid mediators were separated at 50 °C on an Acquity UPLC BEH C18 column (130 Å, 1.7 μm, 2.1 mm × 100 mm, Waters). The Acquity Ultraperformance LC system (Waters) was operated at a flow rate of 0.3 mL/min using a mobile phase consisting of methanol, water, and acetic acid (42:58:0.01, v/v/v), which was ramped to 86:14:0.01 (v/v/v) over 12.5 min followed by isocratic elution at 98:2:0.01 (v/v/v) for 3 min [36]. Eluted lipid mediators were detected by (scheduled) multiple reaction monitoring using a QTRAP 5500 mass spectrometer (Sciex, Framingham, MA), which was equipped with an electrospray ionization source that was operated in negative mode [36,38]. Acquired mass spectra were processed using Analyst 1.6.2 (Sciex).

2.10. Measurement of cell viability

Mitochondrial dehydrogenase activity was assessed by 3-(4,5-dimethylthiazol-2-yl)-2,5-diphenyltetrazolium bromide (Merck) assay as previously reported [31]. Briefly, human monocytes (2×10^5 cells/well) in RPMI 1640 medium supplemented with 10 % FCS, L-glutamine (2 mM), and penicillin/streptomycin (100 U/mL and 100 μg/mL; GE Healthcare) were incubated with vehicle (0.5 % DMSO), test compounds or the pan-kinase inhibitor staurosporine (1 μM, reference compound, Merck) for 24 h at 37 °C and 5 % CO_2. 3-(4,5-Dimethylthiazol-2-yl)-2,5-diphenyltetrazolium bromide (0.5 mg/mL in PBS pH 7.4) was added and the incubation continued for 4 h until purple formazan crystals were clearly visible. After dissolving the formazan product with SDS lysis buffer (10 % in 20 mM HCl, 100 μL) under shaking (≥16 h), absorbance was measured at 570 nm using a Multiskan Spectrum Microplate Reader (Thermo Fisher Scientific, MA, US).

2.11. Determination of radical scavenging activity

Vehicle (ethanol), compound **3b**, cysteine hydrochloride (reference compound, Merck) or ascorbic acid (reference compound, Caesar & Loretz GmbH, Hilden, Germany) were incubated with 2,2-diphenyl-1-picrylhydrazyl (Merck; 50 μM) under shaking in the dark. After 30 min, the absorbance was measured at 520 nm using a Multiskan Spectrum Microplate Reader (Thermo Fisher Scientific) [9].

2.12. Luciferase assays

The NIH-3 T3-KBF-Luc, HaCaT-ARE-Luc, and HeLa-STAT-3-Luc cell lines were previously described [39] and were grown at 37 °C and 5 % CO_2 in supplemented DMEM containing 10 % FBS, 2 mM glutamine, and antibiotics. For the determination of anti-NF-κB activity, NIH-3 T3-KBF-Luc cells were stimulated with TNFα (30 ng/mL) (ImmunoTools, GmbH, Friesoythe, Germany) in the presence or the absence of vehicle, compound **1a** or **3b** for 6 h. Nrf2 activation was analyzed in HaCaT-ARE-Luc cells that were stimulated with vehicle or the compounds for 6 h. To assess anti-STAT3 activity, HeLa-STAT-3-Luc cells were stimulated either with IFN-γ (25 IU/mL) or IL-6 (30 ng/mL) (ImmunoTools GmbH) in the presence or the absence of vehicle or the compounds for 6 h. After the treatment, cells were washed twice in PBS pH 7.4 and lysed in 25 mM Tris-phosphate pH 7.8, 8 mM $MgCl_2$, 1 mM DTT, 1 % Triton X-100, and 7 % glycerol during 15 min at room temperature in a horizontal shaker. Lysates were centrifuged and luciferase activity was measured in the supernatants using a TriStar2 Berthold/LB942 multimode reader (Berthold Technologies GmbH, Bad Wildbad, Germany) following the instructions of the luciferase assay kit (Promega, Madison, WI, USA). The experiments were performed in triplicate and the IC_{50} for NF-κB and STAT3 inhibition and the EC_{50} for Nrf2 were calculated with GraphPad Prism software.

2.13. Statistical analysis

Data are presented as mean ± S.E.M. of *n* observations, where *n* represents the number of independent experiments performed at different time points. The set of compounds was blinded for studies on cell-free 5-LOX and mPGES-1 activity but not for follow-up investigations. Statistical analysis of data was conducted using GraphPad Prism 9 software (San Diego, CA). Data were log-transformed for statistical analysis as indicated. Outliers were identified by a Grubb's test. Paired *t*-tests were applied to compare two groups. For multiple comparisons, repeated measures one-way ANOVA plus Dunnett or Tukeýs *post hoc* tests were used as indicated. *P* values < 0.05 were considered as statistically significant. IC_{50} and EC_{50} values were determined by graphical analysis using GraphPad Prism 9.

3. Results

3.1. Chemistry

Curcumin (**1a**) is usually represented as the linear rotamer of the enolic form, but spectroscopic analyses have highlighted the relevance of bent conformations in solution, as evident from the detection of a major NOESY correlation between the C1 enolic proton and the vinylic $C4^{(,)}$ proton in the ^{1}H- NMR spectra in different solvents [26,40] (Fig. 1**A**). A significant population of twisted conformations of **1a** therefore exists in solution, where rotation around the aryl-olefin bond swaps the orientation of the methoxy compared to the enolic oxygen. Conformational equilibration could play a role in the bioactivity profile of this diarylheptanoid, and to evaluate its biological translation, we have altered the rotational equilibria by introducing substituent(s) on the carbons involved in the process, namely the $C3^{(,)}$ and the aryl *ortho*-positions. This maneuver was applied to four distinct curcuminoid prototypes, namely **1a**, **2a**, and their pyrazole derivatives **3a** and **4a**, all prepared using the Pabon reaction [41] (**Scheme 1**). These changes were expected to affect both the pharmacodynamic [42] and the pharmacokinetic profile of the compounds, since reductive metabolism of curcuminoids by the intestinal microbiota could be altered by increased steric congestion around the β-dicarbonyl group as well as by substitution of the double bonds.

Rotationally constrained curcuminoids (**1b-1e, 2b-2g**) were synthesized by coupling the aryl aldehydes (**5**–**8**) with the 1,3-dicarbonyl (**9**–**13**) under the Pabon bifunctional Claisen-Schmidt strategy

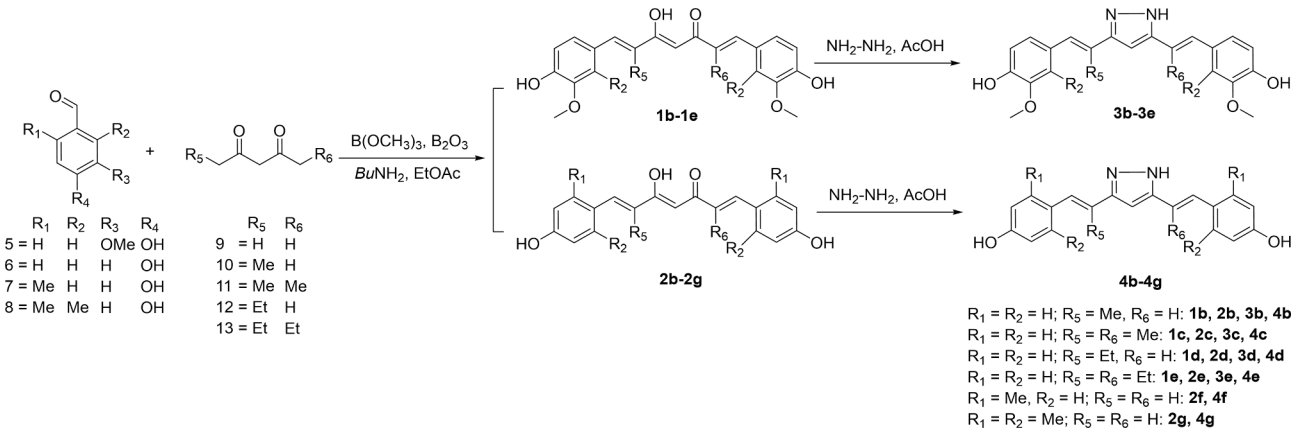

Scheme 1. General preparation of rotational constricted curcuminoids.

(**Scheme 1**, Table 1 [9]). The corresponding pyrazole derivatives (**3b-3e, 4b-4g**) were obtained from **1b** to **1e** or **2b-2g** by treatment with hydrazine in acetic acid. The insertion of a pyrazole moiety is a classic maneuver to raise the structural rigidity and enhance the potency and the selectivity of curcuminoids [9]. We also tried to insert isopropyl groups at C3$^{(')}$ and C4$^{(')}$ of the alkyl linker instead of methyl or ethyl groups, but the reaction failed, probably because the sterically hindered isopropyl residues prevent the reaction between the nucleophilic carbon of the β-diketone system and the electrophilic carbonyl of the aldehyde. The Pabon reaction failed with dicarbonyl compounds bearing branched α-α'-substituents. Therefore, only linear alkyl groups (methyl, ethyl) could be introduced in the C3$^{(')}$ positions.

Table 1
Effect of constrained curcumin derivatives on semi-purified 5-LOX and cell-free mPGES-1 activity.

compound/structure	5-LOX	mPGES-1	Selectivity index[b]	compound/structure	5-LOX	mPGES-1	Selectivity index[b]
curcumin (1a)	0.5 ± 0.0[a]	0.6 ± 0.0[a]	1.2	3c	0.055 ± 0.003	2.30 ± 0.60	41.8
1b	0.221 ± 0.038	2.80 ± 0.20	12.7	3d	0.077 ± 0.007	1.70 ± 0.30	22.1
1c	0.265 ± 0.048	4.20 ± 0.90	15.9	3e	0.079 ± 0.019	2.60 ± 0.30	32.9
1d	0.320 ± 0.102	3.90 ± 0.90	12.2	4a	0.223 ± 0.027	2.10 ± 0.10	9.4
1e	0.124 ± 0.020	2.60 ± 0.60	30.0	4b	0.210 ± 0.020	5.10 ± 1.50	24.3
2a	0.170 ± 0.038	0.16 ± 0.02	0.9	4c	0.213 ± 0.070	1.10 ± 0.00	5.2
2f	0.510 ± 0.048	0.11 ± 0.02	0.2	4d	0.200 ± 0.032	2.10 ± 0.10	10.5
2g	2.334 ± 0.316	1.70 ± 0.10	0.7	4e	0.057 ± 0.015	1.90 ± 0.40	33.3
3a	0.07 ± 0.01[a]	> 10[a]	> 142.9	4f	0.464 ± 0.038	0.70 ± 0.10	1.5
3b	0.038 ± 0.004	1.70 ± 0.10	44.7	4g	0.800 ± 0.097	1.20 ± 0.20	1.5

IC_{50} values (μM) are given as means ± S.E.M. (n = 3). [a]IC_{50} values from reference [9]. [b]Selectivity index = (IC_{50} mPGES-1) / (IC_{50} 5-LOX).

3.2. Impact of rotational constriction on human recombinant 5-LOX and mPGES-1 inhibition

As functional readout, we selected two high-affinity targets of **1a**, i.e., 5-LOX and mPGES-1 [21,25], and evaluated the effect of **1a** and its rotation-restricted derivatives on enzyme activity in cell-free assays (Table 1). Methyl- or ethyl-substitution of **1a** within the linker region (**1b-1e**) enhanced 5-LOX inhibition, with the di-ethylated derivative (**1e**, IC_{50} = 0.124 μM) being most potent (4-fold gain in inhibitory potency vs **1a**). In contrast, alkyl substituents at C3 and C3$^{(')}$ were detrimental for inhibition of mPGES-1 (IC_{50} = 2.60–4.20 μM; **1a**: IC_{50} = 0.6 μM).

Replacement of the 1,3-diketone motif of **1a** with pyrazole dissected mPGES-1 and 5-LOX inhibition, yielding **3a** that selectively inhibits 5-LOX (IC_{50} = 0.07 μM) and is poorly active on mPGES-1 (IC_{50} > 10 μM) [9]. We extended our structure–activity relationship (SAR) study on **3a** and found that respective mono- and di-alkylation of the linker (**3b-3e**) is well tolerated (Table 1). However, only the mono-methylated derivative **3b** (IC_{50} = 0.038 μM, Fig. 1**B**) substantially gains 5-LOX inhibitory activity relative to **3a**. As for mPGES-1, alkylation of **3a** partially restored mPGES-1 inhibition (**3b-3e**: IC_{50} = 1.70–2.60 μM, Table 1).

The natural curcuminoid bisdesmethoxycurcumin (**2a**) is metabolically more stable than **1a** and shows comparable or even superior anti-oxidative, anti-tumoral, and anti-inflammatory effectiveness in various in vitro and in vivo studies [43–46]. Along these lines, **2a** outperformed **1a** in inhibiting cell-free 5-LOX (IC_{50} = 0.170 μM) and mPGES-1 (IC_{50} = 0.16 μM) (Table 1). 5-LOX-inhibitory activity was maintained when the 1,3-diketone of **2a** was replaced by pyrazole (**4a**, IC_{50} = 0.223 μM) but unlike for the other series did not tremendously increase. mPGES-1 is less potently inhibited by the pyrazole analogue **4a** (IC_{50} = 2.10 μM) than by **2a**, as expected. Mono- and di-alkylation of the aryl linker (**4b-4e**) improved 5-LOX inhibition for the di-ethylated derivative **4e**, whereas mono-ethylation (**4d**) and (di)methylation (**4b**, **4c**) were without effect (Table 1). For mPGES-1 inhibition, alkylation of the linker was either detrimental (**4b**), not interfering (**4d**, **4e**), or beneficial in case of dimethylation (**4c**). It seems that the curcuminoid scaffold (**1a**, **2a**, **3a**, **4a**) decides which specific substitution pattern is preferential for 5-LOX inhibition.

As alternative strategy to confine the rotation of the aryl moieties, we introduced a methyl-group into one or both *ortho*-positions of each aromatic ring in **2a** and **4a** yielding **2f**, **2g**, **4f**, and **4g**. *ortho*-methylation was detrimental for 5-LOX inhibition but in particular as 4-hydroxy-2-methyl-phenyl substituents led to more potent mPGES-1 inhibitors (**2f**: IC_{50} = 0.11 μM, **4f**: IC_{50} = 0.70 μM; Table 1). Together, the structure and potentially rigidity of the 1,3-diketone motif (**1a** vs pyrazole series) as well as the strength and likely angle of rotational fixation (mono/di-methylation/ethylation at C3 and C3$^{(')}$) seem to determine 5-LOX and mPGES-1 inhibition by curcuminoids. Manipulation at one site changes the effect of substitutions/replacements at the other. Systematic exploration of rotationally constrained curcuminoids yielded **3b** and **2f** as most potent 5-LOX and mPGES-1 inhibitors, respectively. Further studies addressing the binding mode focused on **3b**.

3.3. Allosteric inhibition of 5-LOX by *3b*

Compound **3b** inhibits semi-purified cell-free 5-LOX independent of the substrate concentration (Fig. 1**C**) and in a reversible manner (Fig. 1**D**), which rather excludes preferential binding to the active site within the arachidonic acid (AA) channel. In line with these findings, compound **3b** (Fig. 1**E**), curcumin (**1a**) (Fig. 1**F**), and the bisdesmethoxy curcuminoid **2f** (Fig. 1**G**) inhibited purified human recombinant 5-LOX largely independent of the AA concentration. The active site iron of 5-LOX undergoes a redox cycle during fatty acid peroxidation, which is blocked by redox-type 5-LOX inhibitors. Compound **3b** (EC_{50} = 27.0 μM) is as efficient in radical scavenging as ascorbic acid or cysteine but does not show anti-oxidant properties at low concentrations (<10 μM) that inhibit 5-LOX (Fig. 1**H**). Our data thus precludes that **3b** non-specifically inhibits 5-LOX through a redox-dependent mechanism.

We recently described an allosteric binding site at the interface of the stable 5-LOX (pdb entry 6NCF) catalytic and regulatory domain that is targeted by boswellic acids [47] and other natural products [34,48]. Molecular docking studies suggest that **3b** binds to this allosteric site, with the phenolic hydroxy group involved in hydrogen bonds to Tyr383 and Asp166 (Fig. 2**A**). An additional hydrogen bond is formed between Arg101 and the pyrazole ring of **3b**. While the curcuminoids displayed a wide variety of possible binding poses, aside from the favored ones shown in Fig. 2**B**, the pyrazolocurcuminoids were conformationally less diverse in the simulation (Fig. 2**A-D**). This finding points towards a more stable energetic minimum for pyrazolocurcuminoids and might explain the superior 5-LOX-inhibitory activity. Compared to curcuminoids, the pyrazole analogs assume a straighter conformation within the binding grove, which seems to be favorable for 5-LOX inhibition (Fig. 2**B**). The C3 methyl group in **3b** further improves the 5-LOX inhibitory activity, likely by filling the binding pocket and generating a favorable tilt of the pyrazole ring that might facilitate the formation of the hydrogen bond with Arg101 (Fig. 2**C**).

Alkylation in both C3 and C3$^{(')}$ position (**3c**, **3e**) does not substantially interfere with the proposed binding mode but is less favorable. Longer alkyl-chains at C3 (e.g., ethyl in **3d**) are also detrimental, possibly because they induce a shift of the contact site due to steric hindrances (Fig. 2**D**). We speculate that the different binding modes of curcuminoids and pyrazolocurcuminoids are the reason why these scaffolds react differently to similar modifications. For example, removing the methoxy groups enhances 5-LOX inhibition in curcuminoids (**2a**) but decreases the inhibitory activity of pyrazolocurcuminoids (**4a**). (Bis)-*ortho*-methylation of the aryl moieties, on the other hand, causes steric hindrance that destabilizes the binding of both scaffolds and is accordingly associated with a strong decrease of 5-LOX inhibition.

Molecular docking studies on mPGES-1 were carried out on the pdb entry 6VL4. The ligand binding site is located between two monomers of the trimeric structure. For mPGES-1, the poses of the curcuminoids (Fig. 2**E**, left panel, **2f**) are very similar to those of the pyrazolocurcuminoids (Fig. 2**E,** right panel, **4f**). Key interactions are hydrogen bonds of the phenolic hydroxy groups with His53 and the surrounding water molecules 318 and 364. The central linker region (either the bis-α, β-unsaturated β-diketone moiety or the pyrazole ring) interact with Tyr130 and water 327 (Fig. 2**E**). The poor mPGES-1-inhibitory activity of pyrazolocurcuminoids cannot be explained from the docking simulation and is likely caused by an effect not related to direct target binding.

3.4. Inhibition of 5-LOX product formation in activated PMNL

Compound **1a** requires substantially higher concentrations to suppress 5-LOX in innate immune cells (PMNL: IC_{50} = 3.9 μM) than to inhibit cell-free 5-LOX (IC_{50} = 0.5 μM) [9]. We therefore investigated the effect of **3b** on 5-LOX product formation in human primary PMNL caused by massive Ca^{2+}-influx. PMNL are major 5-LOX-expressing immune cells that are recruited to sites of inflammation and essentially contribute to LT production during the initiation of inflammation [4]. Compound **3b** effectively inhibited 5-LOX product formation in activated PMNL (IC_{50} = 0.69 μM) (Fig. 3**A**), with comparable potency for the 5-LOX products analyzed, i.e., LTB_4, et-LTB_4, t-LTB_4, and 5-H(p)ETE (Fig. 3**A**). Zileuton, a marketed anti-asthmatic drug that targets 5-LOX [49], was less efficient (Fig. 3**B**). Acute cytotoxic effects of **3b** were not evident within 24 h, as determined in human monocytes by measuring mitochondrial dehydrogenase activity (Fig. 3**C**).

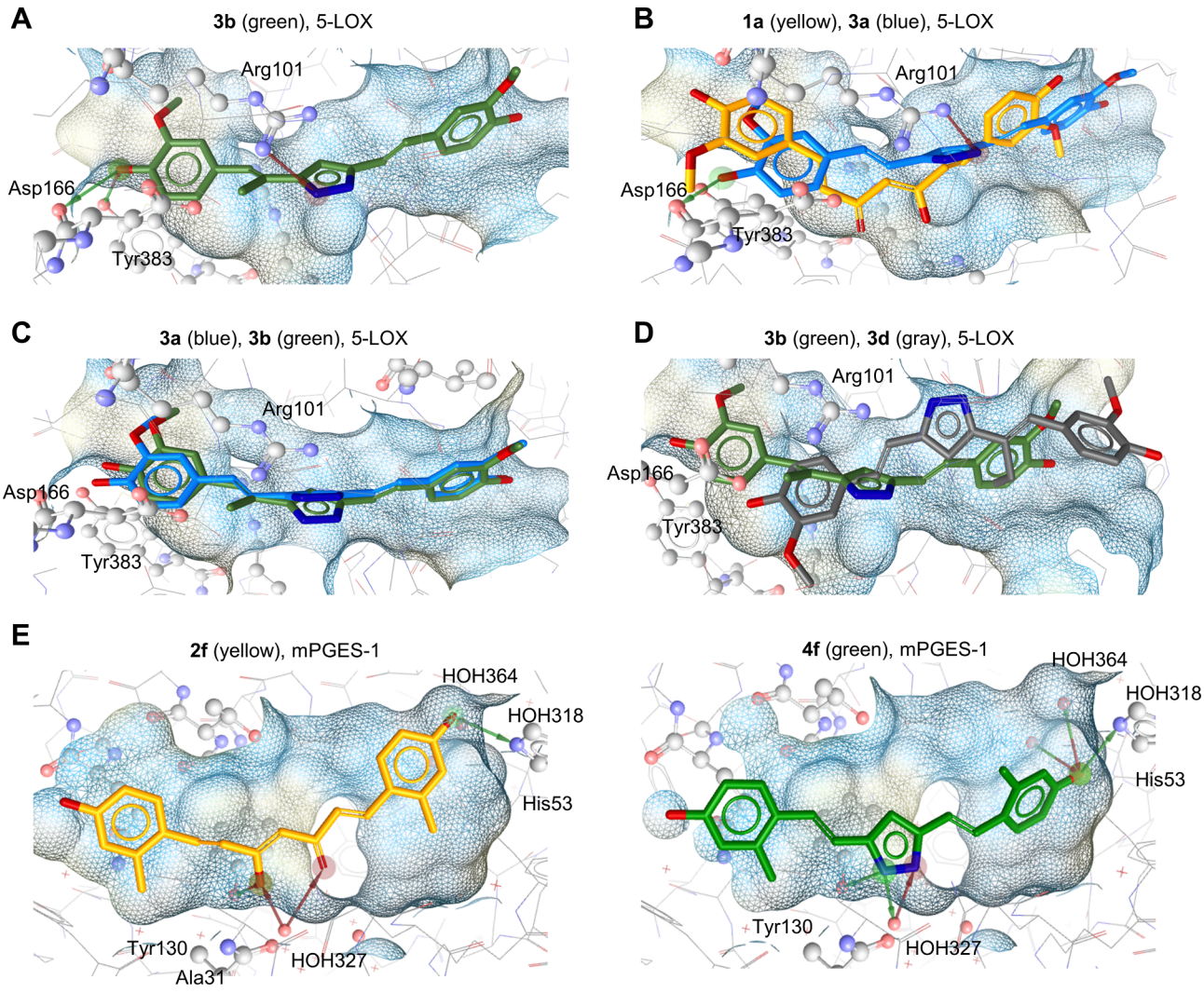

Fig. 2. Molecular binding of curcuminoids with 5-LOX (A-D) and mPGES-1 (E). (A) Binding pose of **3b** (green) in the allosteric binding pocket of 5-LOX. The phenolic hydroxy group forms hydrogen bonds with Tyr383 and Asp166 (green arrow). An additional hydrogen bond is formed between Arg101 and the pyrazole ring (red arrow). (B) Comparison of curcumin (**1a**, yellow) and **3a** (blue). Curcumin assumes a slightly more bent conformation within the binding pocket, while pyrazolocurcumin is sterically restricted and stabilized by an additional hydrogen bond between the pyrazole ring and Arg101. (C) Comparison of **3a** (blue) and **3b** (green). The methylation of C-2 results in a slight tilt of the pyrazole ring. (D) Comparison of **3b** (green) and **3d** (gray). The ethylation of C-2 results in a shift of the molecule within the binding pocket. (E) Molecular binding of the most active curcuminoid **2f** (left, yellow) and pyrazolocurcuminoid **4f** (right, green) in mPGES-1.

3.5. Lipid mediator class switch from LTs to PGs and protectins in macrophages

Inflammation and active resolution involve diverse lipid mediators that display pro-inflammatory and pro-resolving properties [50]. Considering the strong inhibition of LT formation both by isolated 5-LOX and by 5-LOX in PMNL, we next explored the influence of **3b** on the lipid mediator network in human macrophages using a metabololipidomics approach. Focus was placed on M1 macrophages that predominantly produce pro-inflammatory prostaglandins (PG) and LT and M2 macrophages that highly express 15-LOX-1 and generate substantial amounts of specialized pro-resolving mediators (SPM) [35,38]. Monocyte-derived macrophages were polarized to M1 or M2 phenotypes, incubated with **3b** and stimulated with SACM for subsequent lipid mediator profiling [38]. In both macrophage phenotypes, **3b** potently suppressed the formation of LT and other 5-LOX-derived lipid mediators, including 5-HEPE, 5-HETE as well as 5*S*,6*R*-diHETE (Fig. 4**A** and Fig. 4**B**). The availability of polyunsaturated fatty acids that serve as substrates for LM biosynthesis [51] was not impaired.

The drop in 5-LOX products in M2 macrophages was associated with an increase of COX-dependent PG formation (PGE_2, by 6.7-fold) that is too strong as to derive from the re-direction of the 5-LOX substrate AA towards the COX pathway alone. Compound **3b** (at $\geq$ 3 μM) also increased the production of protectins, i.e., PD1 (by 2.8-fold) and PDX (by 2.4-fold), specifically in M2 macrophages, while rather decreasing the formation of resolvins, maresins and lipoxins (Fig. 4**B**). While low concentrations of **3b** (0.3–3 μM) moderately increased the levels of 15-LOX-derived SPM precursors, such as 15-HETE, 15-HEPE, and 14-HDHA, the production of these mediators was reduced at high compound concentrations (30 μM) (Fig. 4**B**). It seems that **3b** shares the weak 12- and 15-LOX inhibitory activity of **1a** [52,53] and analogues [54].

Compound **1a** is a multi-target natural product with diverse bioactivities at micromolar concentrations (10–50 μM). Among others, **1a** inhibits COX isoenzymes [20,21], activates Nrf2 [18], and regulates gene expression via NF-κB [19] and signal transducer and activator of transcription (STAT)3 [22]. We compared the effects of **1a** and **3b** on several of these low-affinity targets to explore whether the rotational restriction of **3b** favors specific target interactions. In fact, **3b** did not activate Nrf2 in reporter gene assays but inhibited STAT3 activation

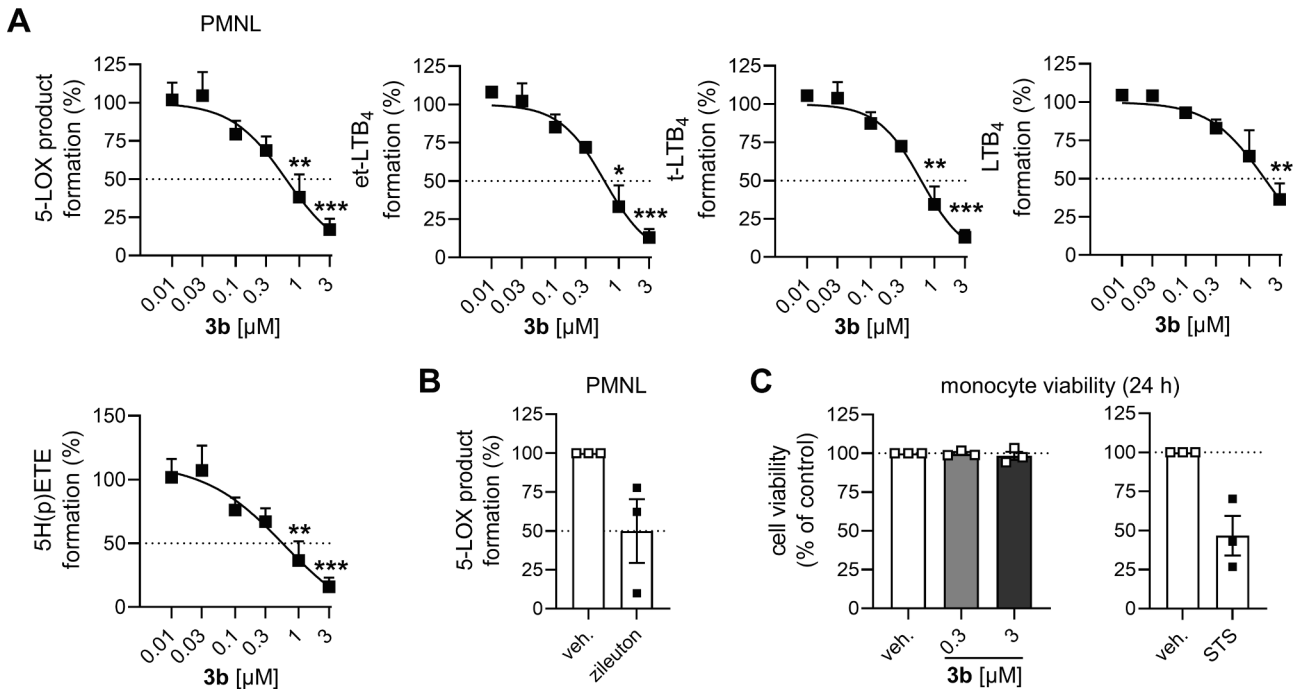

Fig. 3. Compound **3b** inhibits 5-LOX product formation in activated PMNL. (A, B) Effect of **3b** (0.01–3 μM, A) and zileuton (3 μM, B) on human PMNL. 5-LOX product formation was initiated by arachidonic acid (AA, 20 μM) and A23187 (2.5 μM) and 5-LOX products (LTB_4, its isomers et-LTB_4, t-LTB_4, and 5-H(p)ETE) were analyzed by RP-UV-HPLC. (C) Cell viability of monocytes after 24 h of treatment with **3b** (0.3–3 μM); STS, staurosporine (1 μM). H(p)ETE, hydro(pero)xyeicosatetraenoic acid. Results are given as means ± S.E.M., percentage of vehicle control (veh.), n = 3. Absolute values for vehicle control in A-B): 1671 ± 184 pg, 5-LOX products; 145 ± 17 pg, et-LTB_4; 138 ± 20 pg, t-LTB_4; 139 ± 11 pg, LTB_4; 1249 ± 210 pg, 5-H(p)ETE; C) 0.34 ± 0.09 a.u. Data were log-transformed for statistical analysis. ***$p < 0.001$, **$p < 0.01$, *$p < 0.05$ compared to vehicle control; repeated measures one-way ANOVA plus Dunnett's *post hoc* tests.

more potent than **1a** (Table 2).

We observed similar effects on the lipid mediator profile of M1 and M2 macrophages for the rotationally constrained derivative **2f** as for **3b**. Compound **2f** suppressed 5-LOX product formation less potently than **3b**, as expected from the lower inhibitory activity on human recombinant 5-LOX, but was more effective in inducing PG and SPM production (Fig. 5). Note that levels of PGE_2 (12-fold) experienced a stronger increase than those of protectins (2-fold) in M2 macrophages. Levels of SPM precursors and SPM already increased for low **2f** concentrations (0.3–3 μM). The upregulation of SPM and its precursors was especially prominent in M1 macrophages, which are otherwise poor sources for 12/15-LOX-derived LM. Despite potent inhibition of mPGES-1 in microsomal preparations, **2f** did not lower PGE_2 synthesis in M1 macrophages (Fig. 5). Together, **3b** and **2f** trigger a lipid mediator class switch from 5-LOX-derived LT towards PGs and SPM in human macrophages, with different pharmacodynamics and efficiency for individual LM classes.

4. Discussion

Because of a pleiotropic profile of targets, a modest affinity of binding, and substantially flat SARs, curcumin (**1a**) has been viewed as a PAIN or, alternatively, as a privileged unfocused platform for the induction of bioactivity [55]. On the other hand, **1a** can also inhibit with high-affinity a few specific targets, which qualifies it as a mainstream structure for drug discovery. Within these high-affinity targets, 5-LOX and mPGES-1 [1,21,25] are relevant for their key role in the biosynthesis of pro-inflammatory LTs and of PGE_2, [1]. In previous work, we have shown that 5-LOX and mPGES-1 inhibition by curcuminoids can be dissected by point-like mutations like aryl-prenylation [21,22], shortening of the alkyl linker chain [8], and modification of the 1,3-dicarbonyl system [9,10]. Rotation around the vinyl bonds is responsible for the interconversion of linear and twisted conformations of **1a** and for the attainment of distinct orientations of the methoxy and the enolic oxygen. Since the biological translation of this conformational mobility is unknown, we have investigated how the perturbation of the rotameric equilibration of **1a** differentially affects its 5-LOX and mPGES-1 inhibition profile. These insights eventually led to the discovery of dual 5-LOX/mPGES-1 inhibitors with either selectivity for 5-LOX (**3b**; 44.7-fold) or mPGES-1 (**2f**; 4.6-fold). Both compounds trigger a lipid mediator class switch from pro-inflammatory LTs to PG and SPM in activated human macrophage subtypes. While we consider dual inhibition of 5-LOX and mPGES-1 to be favorable for most therapeutic applications, there are also niches for selective inhibitors. For example, PGE_2 has bronchodilatory properties in normal subjects [56] as well as patients with asthma and chronic bronchitis [57]. Therefore, under such pathological conditions, inhibitors with a higher selectivity of 5-LOX over mPGES-1 might be preferred, in particular when raising PGE_2 and SPM levels.

Extensive SAR studies have been carried out on the anti-inflammatory activity of curcuminoids, but the relevance of the conformational flexibility of the lead structure has remained substantially unknown [58]. The strategy we have followed to perturbate the rotameric equilibration of **1a** around its vinylic bonds capitalizes on the buttressing effect of alkyl groups located at the carbons pivotal to rotable sigma bonds ($C3^{(,)}$ for the carbonyl-$C3^{(,)}$ bond, the two aryl *ortho*-positions for the aryl-$C4^{(,)}$ bond). This maneuver was carried out on four curcuminoid structural primers, namely **1a**, bisdesmethoxycurcumin (**2a**) and their pyrazole isosters (**3a**, **4a**). Compound **2a** is a natural component of the curcuminoid bouquet to turmeric. It has been reported to be chemically more stable than **1a** [59], although the instability of **2a** seems to have be largely overemphasized in the literature [60]. Compared to **2a**, compound **1a** shows weaker antioxidant [61] and anti-inflammatory activities [43,46], using as end-points NF-κB activation and COX-2 inhibition. Conversely, **2a** is more effective than **1a** in inhibiting 5-LOX and mPGES-1, a finding in line with the pronounced anti-inflammatory activity of **2a** in carrageenan-induced paw edema in mice [62] and rats [63], where the enrichment of **2a** in the turmeric

A

0 100 250
[% of veh.]

		M1 (veh.)	3b 0.3 μM	%	3 μM	%	30 μM	%
5-LOX	5-HEPE	248 ± 91	178 ± 26	72	94 ± 38	38	56 ± 9	23
	5-HETE	2308 ± 940	1518 ± 454	66	473 ± 158	21	193 ± 9	8
	t-LTB$_4$	213 ± 86	162 ± 60	76	60 ± 35	28	6 ± 0	3
	LTB$_4$	801 ± 430	641 ± 233	80	152 ± 69	19	6 ± 0	1
	5S,6R-diHETE	88 ± 34	70 ± 22	79	23 ± 9	26	5 ± 2	6
COX	PGE$_2$	9211 ± 189	9359 ± 384	102	7348 ± 859	80	10774 ± 518	117
	PGD$_2$	221 ± 16	209 ± 19	95	185 ± 22	84	505 ± 45	229
	PGF$_{2\alpha}$	882 ± 242	972 ± 241	110	988 ± 272	112	1663 ± 397	189
	TXB$_2$	11368 ± 1024	13033 ± 1013	115	13016 ± 1461	115	6348 ± 603	56
SPM precursors	17-HDHA	1987 ± 359	1919 ± 622	97	1736 ± 728	87	2294 ± 875	115
	14-HDHA	112 ± 20	99 ± 12	89	82 ± 2	73	87 ± 4	78
	7-HDHA	82 ± 16	64 ± 8	77	42 ± 7	51	35 ± 4	42
	4-HDHA	76 ± 16	68 ± 8	89	58 ± 5	77	58 ± 4	76
12/15-LOX	15-HEPE	156 ± 26	185 ± 83	118	147 ± 60	94	216 ± 99	138
	12-HEPE	21 ± 4	21 ± 3	103	21 ± 3	103	21 ± 4	103
	15-HETE	3240 ± 393	3459 ± 781	107	2934 ± 982	91	4152 ± 1356	128
	12-HETE	140 ± 26	134 ± 9	95	109 ± 16	78	120 ± 7	86
	5,15-diHETE	115 ± 30	72 ± 14	63	50 ± 13	43	26 ± 7	23
SPM	PD1	17 ± 0	14 ± 1	82	11 ± 0	64	11 ± 1	65
	PDX	8 ± 1	7 ± 1	96	5 ± 1	72	5 ± 1	62
	RvD5	10 ± 1	9 ± 1	89	5 ± 1	49	4 ± 0	41
	MaR1	3 ± 1	2 ± 1	79	2 ± 0	61	1 ± 1	57
	LXA$_4$	7 ± 0	7 ± 0	94	6 ± 0	77	6 ± 1	76
PUFAs	AA	119233 ± 21828	113532 ± 1890	95	130702 ± 12879	110	136346 ± 16486	114
	EPA	30608 ± 3416	27125 ± 2316	89	29966 ± 1997	98	35816 ± 3853	117
	DHA	95384 ± 21677	93944 ± 15195	98	111932 ± 16123	117	109200 ± 20842	114

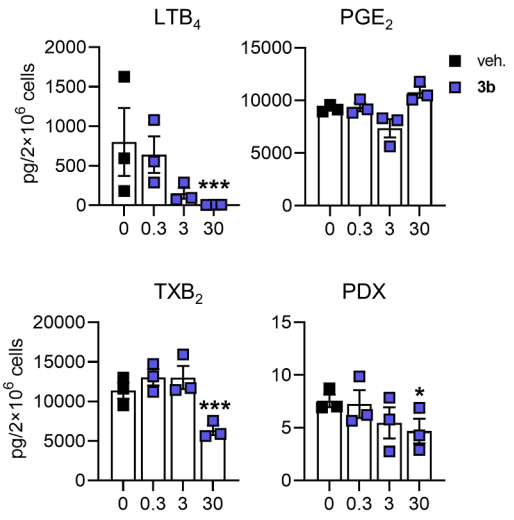

B

0 100 250
[% of veh.]

		M2 (veh.)	3b 0.3 μM	%	3 μM	%	30 μM	%
5-LOX	5-HEPE	217 ± 86	174 ± 42	80	83 ± 8	38	35 ± 6	16
	5-HETE	2683 ± 1380	1563 ± 707	58	630 ± 280	23	197 ± 21	7
	t-LTB$_4$	181 ± 90	119 ± 49	66	63 ± 32	35	23 ± 5	13
	LTB$_4$	388 ± 244	281 ± 158	72	138 ± 106	36	14 ± 4	4
	5S,6R-diHETE	114 ± 70	66 ± 39	58	31 ± 23	27	5 ± 1	4
COX	PGE$_2$	467 ± 138	460 ± 109	99	637 ± 145	137	3136 ± 194	672
	PGD$_2$	134 ± 37	130 ± 25	97	161 ± 39	120	676 ± 72	505
	PGF$_{2\alpha}$	478 ± 220	452 ± 179	95	554 ± 212	116	1762 ± 512	369
	TXB$_2$	16303 ± 5831	15963 ± 4694	98	17352 ± 5688	106	11167 ± 3503	68
SPM precursors	17-HDHA	16527 ± 4905	17801 ± 5371	108	14150 ± 4125	86	10210 ± 4185	62
	14-HDHA	1513 ± 562	1612 ± 510	107	1717 ± 494	113	1520 ± 753	100
	7-HDHA	238 ± 38	250 ± 52	105	288 ± 54	121	214 ± 70	90
	4-HDHA	83 ± 4	75 ± 10	90	69 ± 4	82	59 ± 4	71
12/15-LOX	15-HEPE	1882 ± 616	3209 ± 1170	171	2346 ± 847	125	1449 ± 730	77
	12-HEPE	222 ± 80	325 ± 112	146	297 ± 107	134	174 ± 88	78
	15-HETE	23338 ± 4889	29248 ± 6290	125	23452 ± 5222	100	18023 ± 6941	77
	12-HETE	1330 ± 339	1442 ± 304	108	1468 ± 260	110	1202 ± 504	90
	5,15-diHETE	724 ± 235	450 ± 55	62	194 ± 51	27	55 ± 13	8
SPM	PD1	24 ± 4	26 ± 4	107	36 ± 7	152	68 ± 28	284
	PDX	33 ± 12	32 ± 8	96	47 ± 12	142	80 ± 31	239
	RvD5	395 ± 196	385 ± 148	97	344 ± 129	87	167 ± 91	42
	MaR1	47 ± 20	43 ± 10	91	47 ± 15	101	35 ± 15	75
	LXA$_4$	10 ± 2	8 ± 0	80	7 ± 1	69	6 ± 0	56
PUFAs	AA	135294 ± 9489	156075 ± 15735	115	134677 ± 17942	100	156349 ± 29216	116
	EPA	37757 ± 10660	30329 ± 3127	80	29122 ± 1742	77	42925 ± 7246	114
	DHA	83918 ± 7433	97006 ± 8971	116	89122 ± 17232	106	97659 ± 19304	116

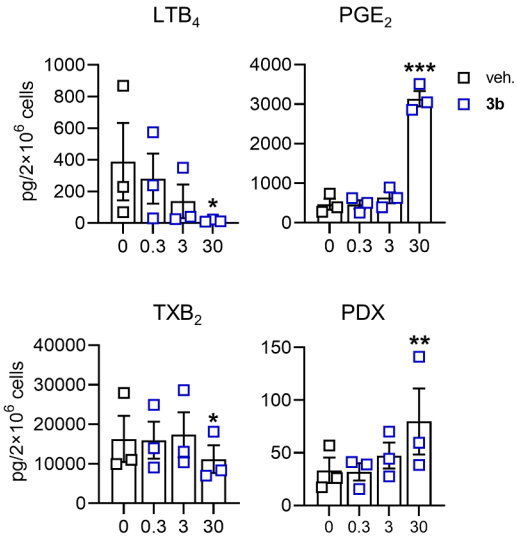

Fig. 4. Compound **3b** triggers a lipid mediator class switch from 5-LOX metabolites to prostaglandins and SPM in macrophages. (A, B) Human macrophages of the M1 (A) and M2 phenotype (B) were pre-treated with **3b** for 15 min and then stimulated with SACM for 180 min, and lipid mediator profiles were determined by UPLC-MS/MS. The color scheme of the heatmaps shows the mean percentage change upon treatment with **3b** (0.3–30 μM) relative to vehicle control (veh.). Data are given as pg lipid mediator / 2×10^6 cells or percentage of control as indicated. (di)HEPE, (di)hydroxy-eicosapentaenoic acid; (di)HETE, (di)hydroxy-eicosatetraenoic acid; HDHA, hydroxy-docosahexaenoic acid; LX, lipoxin; AA, arachidonic acid; EPA, eicosapentaenoic acid; DHA, docosahexaenoic acid. Bar charts show selected lipid mediators as means ± S.E.M., n = 3. Data were log-transformed for statistical analysis. ***$p < 0.001$, **$p < 0.01$, *$p < 0.05$ compared to vehicle control; repeated measures one-way ANOVA plus Dunnett's *post hoc* tests.

extract from 3.6 % to 70 % was shown to enhance efficiency. Little is known about pyrazolocurcuminoids, except that **3a** potently inhibits 5-LOX but hardly affects mPGES-1 [9]. Here, we show that the balance between 5-LOX and mPGES-1 inhibition is partially restored for the corresponding bisdesmethoxy derivative **4a**, due to impaired 5-LOX- and enhanced mPGES-1-inhibitory activity relative to **3a**.

SARs for modifications that constrain the conformation of curcuminoids are complex: methyl or -ethyl substituents on C3$^{(\cdot)}$ improve 5-LOX inhibition for **1a** (compounds **1b-1e**) but not for its pyrazole derivative (compounds **3b-3e**) or the bisdesmethoxy-pyrazolocurcuminoid scaffold **4a** (compounds **4b-4e**). For mPGES-1 activity, the rotationally constriction around the carbonyl-C3$^{(\cdot)}$ bond was beneficial in case of the pyrazole framework (**4b-4e**) but detrimental for **1a** itself (**1b-1e**). Remarkably, C3$^{(\cdot)}$-methylation (**1c**) has been reported to increase the anti-angiogenic activity of **1a** [42] resulting in more potent inhibition of NF-κB transcriptional activity [64]. The former was ascribed to an impaired reductive metabolism of the parent compound by alcohol dehydrogenase and a more pronounced inhibitory effect on the

Table 2
Effect of compound **3b** and **1a** on Nrf2, NF-κB and STAT3 transcriptional activities.

compound / structure	Nrf2[a]	NF-κB[b] (TNF-α)	STAT3[b] (IFNγ)	STAT3[b] (IL6)
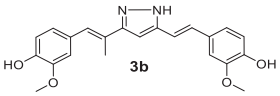 **3b**	> 25	> 25	29.70 ± 0.11	6.7 ± 6.3
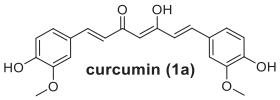 **curcumin (1a)**	5.70 ± 0.15	30.2 ± 4.8	> 25	33.2 ± 8.1

[a] EC_{50} values (μM) were calculated as concentrations to achieve half-maximal Nrf2 activation by *tert*-butylhydroquinone (20 μM). [b]IC_{50} values (μM) are given as means ± SEM of single determinations obtained in three independent experiments.

phosphorylation of extracellular signal-regulated kinase-1/2 and vascular endothelial growth factor receptor [42]. In turn, this was suggested to depend on the conversion of 3,3'-dimethyl-curcumin (**1c**) into its corresponding epoxide or into a chain-shortened alcohol, which then inhibits NF-κB activation through covalent adduction to Cys179 of inhibitor of NF-κB kinase (IKK)β [64].

How aryl substitution of **1a** influences the activity against pro-inflammatory targets has been previously investigated: *m*, *m*'-diprenylation diminishes mPGES-1 rather than 5-LOX inhibition [6,9], while the introduction of halogens (i.e., Cl, Br, F) at C9 and C9(') was without effect on the suppression of NF-κB signaling [46]. We excluded rotational constriction as central driver of SARs in these series because substituents were placed in *meta*-position. Note that studies on rotationally restricting *ortho*-modifications are rather limited for curcuminoids. Ahmad et al. [65] and Lee et al. [66] explored for multiply substituted and truncated diarylpentanoid curcuminoids how *ortho*-substitution with methyl or methoxy groups influences the inhibition of pro-inflammatory pathways. Compared to **1a**, *o*-methyl/*p*-diethylaminoacetonitrile derivatives were more effective in inhibiting secretory phospholipase A_2, COX-1/2 and soybean LOX but failed to enhance mPGES-1 inhibition [65]. Superior suppression of iNOS-dependent NO production was evident for *o*-methoxy derivatives [66]. In our hands, *ortho*-methylation of the phenol moiety in **2a** and **4a** attenuated the inhibition of human 5-LOX and enhanced the mPGES-1-inhibitory activity, in particular for *o*, *o*'-dimethylation. The systematic investigation of rotational constriction via *o*-aryl substitutions led to **2f** (IC_{50} = 0.11 μM), the most potent mPGES-1 inhibitor within the here investigated curcuminoid series.

The molecular interactions that may underlie these complex SARs were explored for stable 5-LOX and mPGES-1 using a molecular docking approach. The studies on the 5-LOX allosteric binding site can explain the potent 5-LOX inhibition by pyrazolocurcuminoids and rationalize the impact of concrete modifications. The docking workflow can therefore be used to meaningfully evaluate these and future curcuminoid derivatives. However, the molecular discriminants that define mPGES-1 inhibition remained enigmatic, possibly due to effects unrelated to direct ligand target binding, such as access of the ligand to the binding pocket via the membrane.

Compound **1a** and other curcuminoids have been proposed to bind close to the active site iron of soybean LOX-3 in a non-competitive manner [67] and form hydrophobic or π-π interactions with soybean LOX-3 or human P-12-LOX [54,68–70]. While these LOX enzymes share a conserved core domain with human 5-LOX, in which the catalytic iron is surrounded by a bundle of helices [71], the latter has a distinct active site due to the unique orientation of helix α2 that modulates access to the catalytic iron [72]. Since human 5-LOX inhibition by **1a**, **3b** and **2f** is not or hardly affected by the AA concentration, we do not consider the active site as preferred target of curcuminoids but favor the here proposed allosteric site. However, further clarification is needed about whether the weak trend towards higher IC_{50} values at high AA concentrations indicates a dual inhibitory mode, involving partial binding to the active site. In further support of this hypothesis, **3b** exhibits weak radical scavenging activity, which does not qualify for redox-inhibition at the catalytic site, unless specific protein binding increases the redox potential.

To assess the anti-inflammatory activities of the rotationally restrained curcuminoids, we investigated the effect of **3b** (the most potent 5-LOX inhibitor) and **2f** (which excels in mPGES-1 inhibition) on lipid mediator biosynthesis in human macrophages. Both compounds favorably induced a lipid mediator class switch from pro-inflammatory LTs to PG and SPM. The latter are pivotal pro-resolving mediators that inhibit neutrophil infiltration, stimulate phagocytosis of debris and accelerate tissue repair at low effective concentrations [73]. Protectins, for example, suppress PMNL infiltration in vitro at 1–100 nM and in vivo at 0.01–100 ng/mouse [74]. Whether relevant concentrations are reached in specific physiological contexts, however, requires further investigation, as does the elucidation of the exact mechanisms [75]. Along the lines, **1a** has recently been shown to modulate macrophage polarization and promote osteogenic differentiation and bone regeneration [76]. We speculated that **3b** alters the regional specificity of 5-LOX towards oxygenation of AA and EPA at C12 and C15, and DHA at C14 and C17, as previously described for AKBA [47], thereby circumventing the need for 15-LOX in SPM biosynthesis. However, neither **1a**, **3b** nor **2f** enable human recombinant 5-LOX to efficiently convert AA into 12- or 15-HETE (data not shown). Compounds **3b** and **2f** elevated the production of protectins but not RvD5 or LXA_4 in M2 macrophages. The latter is likely a consequence of the potent inhibition of 5-LOX activity, which participates in the biosynthesis of RvD5 and LXA_4 [50]. Of interest in this context is also that **2f** strongly elevates the levels of monohydroxylated 12- and 15-LOX products in activated M2 macrophages, whereas **3b** has a weak suppressive effect, which might be explained by a moderate inhibition of 12-LOX and 15-LOX isoenzymes. On the other hand, both **3b** and **2f** substantially upregulate protectin levels, which rather excludes that activation or induction of 12/15-LOX drives the lipid mediator class switch. The underlying mechanisms remain enigmatic but might rely on the subcellular distribution of LOX isoenzymes or their functional coupling with phospholipase A_2 isoenzymes and terminal hydrolases. Notably, the effects on monohydroxylated 12/15-LOX products seem also to be concentration- and cell type-specific. Thus, low concentrations of **3b** (0.3 μM) elevate the levels of specific 12/15-LOX products in M2 macrophages but decrease them at higher concentrations (3 μM) (Fig. 4**B**), whereas, in PMNL, compound **3b** triggers 15-HETE (but not 12-HETE) production (142 % of vehicle control at 0.3 μM; 202 % of vehicle control at 3 μM; data not shown). Monitoring intracellular curcuminoid concentrations might be essential for unraveling this complex profile. Together, curcuminoids can be added to the small number of natural products that shift lipid mediator generation from pro-inflammatory 5-LOX products towards SPM [31,48,77], although the detailed mechanisms remain enigmatic.

SPM biosynthesis in **3b**- or **2f**-pre-treated macrophages was accompanied by an increased abundance of prostanoids. Although the exact underlying mechanisms are not fully understood, it is remarkable that the levels of the COX product TXB_2 decreased (at 30 μM), which points towards subordinate targets of **3b** such as COX-1 or thromboxane synthase. In fact, COX-1 has previously been reported as moderate target of **1a** and diverse derivatives [9,20]. Moreover, we were surprised that the dual 5-LOX/mPGES-1 inhibitors **3b** and **2f** potently inhibited mPGES-1 in a cell-free assay, but neither reduced PGE_2 levels in human M1 macrophages that, in contrast to M2, express abundant mPGES-1. We assume that mPGES-1 inhibition is overcompensated by an overall increase of PG biosynthesis. In support of this hypothesis, **2f** prevented the expected upregulation of PGE_2 in M1 macrophages, an effect that is selective for PGE_2, while the concentrations of other PGs, i.e., PGD_2 and

A

0 100 250
[% of veh.]

		M1 (veh.)	2f 0.3 μM	%	2f 3 μM	%	2f 30 μM	%
5-LOX	5-HEPE	248 ± 91	223 ± 40	90	167 ± 64	67	57 ± 8	23
	5-HETE	2308 ± 940	2064 ± 918	89	1056 ± 329	46	348 ± 60	15
	t-LTB$_4$	213 ± 86	228 ± 88	107	152 ± 72	71	13 ± 3	6
	LTB$_4$	801 ± 430	883 ± 450	110	672 ± 319	84	22 ± 3	3
	5S,6R-diHETE	88 ± 34	97 ± 37	110	31 ± 9	35	6 ± 1	7
COX	PGE$_2$	9211 ± 189	9158 ± 483	99	9304 ± 695	101	10168 ± 1517	110
	PGD$_2$	221 ± 16	229 ± 28	104	268 ± 7	121	508 ± 100	230
	PGF$_{2\alpha}$	882 ± 242	982 ± 267	111	987 ± 203	112	1810 ± 319	205
	TXB$_2$	11368 ± 1024	12382 ± 699	109	9213 ± 962	81	1546 ± 70	14
SPM precursors	17-HDHA	1987 ± 359	3100 ± 1251	156	3752 ± 1671	189	6822 ± 2377	343
	14-HDHA	112 ± 20	146 ± 27	130	131 ± 3	117	158 ± 21	141
	7-HDHA	82 ± 16	180 ± 91	218	72 ± 9	88	55 ± 7	67
	4-HDHA	76 ± 16	83 ± 11	109	81 ± 13	106	87 ± 4	114
12/15-LOX	15-HEPE	156 ± 26	314 ± 159	201	384 ± 188	245	699 ± 212	447
	12-HEPE	21 ± 4	41 ± 13	197	33 ± 5	157	36 ± 6	175
	15-HETE	3240 ± 393	4791 ± 1737	148	5705 ± 2235	176	15824 ± 3696	488
	12-HETE	140 ± 26	188 ± 36	134	203 ± 28	145	301 ± 46	215
	5,15-diHETE	115 ± 30	210 ± 120	183	626 ± 464	546	3753 ± 29	3271
SPM	PD1	17 ± 0	27 ± 8	158	32 ± 5	192	25 ± 5	148
	PDX	8 ± 1	14 ± 4	187	26 ± 3	340	20 ± 4	263
	RvD5	10 ± 1	35 ± 22	348	9 ± 1	91	10 ± 1	97
	MaR1	3 ± 1	4 ± 0	151	2 ± 0	65	2 ± 0	72
	LXA$_4$	7 ± 0	33 ± 26	452	10 ± 1	135	14 ± 1	196
PUFAs	AA	119233 ± 21828	125480 ± 28932	105	152069 ± 10472	128	130012 ± 3498	109
	EPA	30608 ± 3416	24024 ± 1609	78	30672 ± 5285	100	26258 ± 2143	86
	DHA	95384 ± 21677	113902 ± 38437	119	127804 ± 12137	134	85832 ± 7210	90

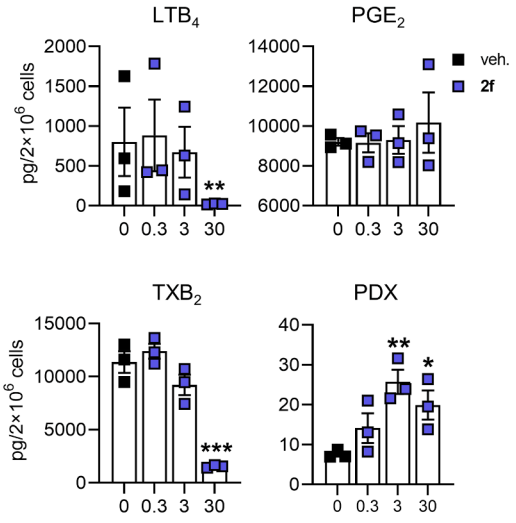

B

0 100 250
[% of veh.]

		M2 (veh.)	2f 0.3 μM	%	2f 3 μM	%	2f 30 μM	%
5-LOX	5-HEPE	217 ± 86	243 ± 83	112	164 ± 66	75	60 ± 15	28
	5-HETE	2683 ± 1380	2479 ± 1079	92	1888 ± 1182	70	620 ± 218	23
	t-LTB$_4$	181 ± 90	211 ± 86	117	222 ± 132	123	39 ± 17	21
	LTB$_4$	388 ± 244	462 ± 214	119	748 ± 601	193	52 ± 33	13
	5S,6R-diHETE	114 ± 70	85 ± 39	74	54 ± 34	47	8 ± 3	7
COX	PGE$_2$	467 ± 138	625 ± 140	134	1979 ± 639	424	5578 ± 3002	1196
	PGD$_2$	134 ± 37	168 ± 36	125	389 ± 122	290	1085 ± 611	810
	PGF$_{2\alpha}$	478 ± 220	588 ± 225	123	1083 ± 476	227	3505 ± 2028	734
	TXB$_2$	16303 ± 5831	17955 ± 5144	110	14628 ± 6436	90	1214 ± 645	7
SPM precursors	17-HDHA	16527 ± 4905	17884 ± 6778	108	19523 ± 5726	118	19207 ± 6847	116
	14-HDHA	1513 ± 562	1752 ± 729	116	1907 ± 595	126	1878 ± 575	124
	7-HDHA	238 ± 38	250 ± 69	105	222 ± 46	93	157 ± 43	66
	4-HDHA	83 ± 4	72 ± 7	86	94 ± 3	113	95 ± 18	115
12/15-LOX	15-HEPE	1882 ± 616	2596 ± 1051	138	3590 ± 1235	191	6128 ± 3718	326
	12-HEPE	222 ± 80	299 ± 111	135	348 ± 107	157	475 ± 272	214
	15-HETE	23338 ± 4889	27544 ± 7362	118	37673 ± 7755	161	75145 ± 37574	322
	12-HETE	1330 ± 339	1680 ± 495	126	2144 ± 320	161	4039 ± 1541	304
	5,15-diHETE	724 ± 235	662 ± 102	91	1118 ± 162	155	5651 ± 2903	781
SPM	PD1	24 ± 4	24 ± 6	101	53 ± 11	222	41 ± 14	170
	PDX	33 ± 12	38 ± 11	115	69 ± 22	207	56 ± 19	168
	RvD5	395 ± 196	393 ± 186	99	604 ± 296	153	315 ± 166	80
	MaR1	47 ± 20	51 ± 19	109	85 ± 34	181	58 ± 23	122
	LXA$_4$	10 ± 2	10 ± 1	102	13 ± 1	129	15 ± 5	149
PUFAs	AA	135294 ± 9489	153235 ± 17583	113	155277 ± 26142	115	164047 ± 25649	121
	EPA	37757 ± 10660	35811 ± 5042	95	29255 ± 2676	77	32973 ± 5925	87
	DHA	83918 ± 7433	92657 ± 7163	110	92068 ± 19317	110	78539 ± 8253	94

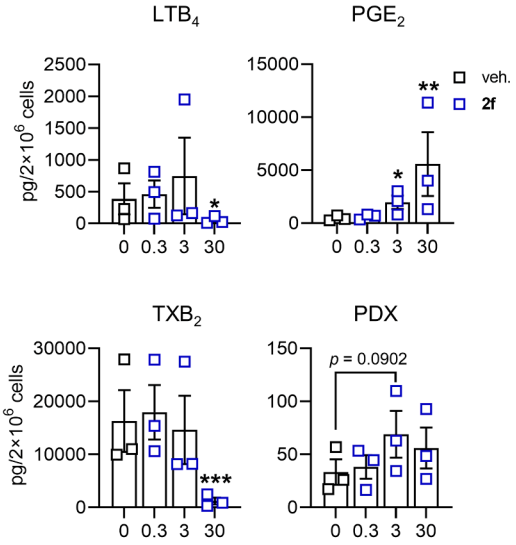

Fig. 5. Effect of compound **2f** on the lipid mediator profile of human M1 and M2 macrophages. (A, B) Human macrophages of the M1 (A) and M2 phenotype (B) were pre-treated with **3b** for 15 min and then stimulated with SACM for 180 min, and lipid mediator profiles were determined by UPLC-MS/MS. The color scheme of the heatmaps shows the mean percentage change upon treatment with **2f** (0.3–30 μM) relative to vehicle control (veh.). Data are given as pg lipid mediator / 2 × 10^6 cells or percentage of control as indicated. (di)HEPE, (di)hydroxy-eicosapentaenoic acid; (di)HETE, (di)hydroxy-eicosatetraenoic acid; HDHA, hydroxy-docosahexaenoic acid; LX, lipoxin; AA, arachidonic acid; EPA, eicosapentaenoic acid; DHA, docosahexaenoic acid. Bar charts show selected lipid mediators as mean ± S.E.M., n = 3. Data were log-transformed for statistical analysis. ***$p < 0.001$, **$p < 0.01$, *$p < 0.05$ compared to vehicle control; repeated measures one-way ANOVA plus Dunnett's *post hoc* tests.s

$PGF_2\alpha$, were elevated. The less potent mPGES-1 inhibitor **3b** did instead not effectively buffer the increase of PGE_2 levels. Note that PGE_2, depending on its spatial and temporal distribution, displays both pro-inflammatory and anti-inflammatory functions. Mechanistically, PGE_2 is important for triggering the lipid mediator class switch from pro-inflammatory LTs to LXA_4, which limits the inflammatory reaction and promotes resolution [78]. Elevated PGE_2 levels, in combination with increased SPM production, are therefore not necessarily detrimental but might even contribute to the anti-inflammatory activity of the curcuminoids.

In summary, we have designed, synthesized and biologically evaluated a library of conformationally constricted curcuminoids, substituted at critical positions to affect the rotational equilibration between linear and bent geometries and between *syn*- and *anti*-orientations of the carbonyl and methoxy oxygen atoms. We have identified the structural features underlying the dissection of 5-LOX and mPGES-1 inhibition, and validated the potential as drug candidates of two compounds capable to induce a switch from pro-inflammatory LTs to PGs and SPMs

while, at the same time, buffering PGE_2 biosynthesis.

CRediT authorship contribution statement

Zhigang Rao: Investigation, Writing – original draft, Formal analysis, Validation, Funding acquisition. **Diego Caprioglio:** Investigation, Writing – review & editing. **André Gollowitzer:** Investigation, Validation, Formal analysis, Writing – review & editing. **Christian Kretzer:** Investigation, Formal analysis. **Daniela Imperio:** Investigation. **Juan A. Collado:** Investigation. **Lorenz Waltl:** Investigation, Writing – review & editing. **Sandra Lackner:** Investigation, Validation, Writing – review & editing. **Giovanni Appendino:** Conceptualization, Writing – review & editing. **Eduardo Muñoz:** Methodology, Writing – review & editing. **Veronika Temml:** Investigation, Writing – review & editing, Validation, Funding acquisition. **Oliver Werz:** Methodology, Writing – review & editing, Funding acquisition. **Alberto Minassi:** Conceptualization, Resources, Writing – original draft, Project administration, Data curation, Supervision. **Andreas Koeberle:** Conceptualization, Resources, Writing – original draft, Project administration, Data curation, Supervision, Funding acquisition.

Declaration of Competing Interest

The authors declare that they have no known competing financial interests or personal relationships that could have appeared to influence the work reported in this paper.

Data availability

Data will be made available on request.

Acknowledgements

The authors thank Katrin Fischer, Monika Listing, Bärbel Schmalwasser and Saskia Schmidt for technical assistance in performing experiments.

This research was funded in part by the Austrian Science Fund (FWF) (I4968-B), the Tyrolean Science Fund (TWF) (F.33467/7-2021), Bionorica Research GmbH (project number 320092), Deutsche Forschungsgemeinschaft (DFG) and Collaborative Research Center SFB 1278 “PolyTarget” (project number 316213987, project A04). V.T. was funded by the Austrian Science Fund (FWF) project T942. For the purpose of open access, the author has applied a CC BY public copyright license to any Author Accepted Manuscript version arising from this submission.

References

[1] A. Koeberle, O. Werz, Natural products as inhibitors of prostaglandin E2 and pro-inflammatory 5-lipoxygenase-derived lipid mediator biosynthesis, Biotechnol. Adv. 36 (6) (2018) 1709–1723, https://doi.org/10.1016/j.biotechadv.2018.02.010.

[2] A. Koeberle, O. Werz, Multi-target approach for natural products in inflammation, Drug Discov. Today 19 (12) (2014) 1871–1882, https://doi.org/10.1016/j.drudis.2014.08.006.

[3] O. Rådmark, O. Werz, D. Steinhilber, B. Samuelsson, 5-Lipoxygenase, a key enzyme for leukotriene biosynthesis in health and disease, Biochim. Biophys. Acta 1851 (4) (2015) 331–339, https://doi.org/10.1016/j.bbalip.2014.08.012.

[4] M. Peters-Golden, W.R. Henderson Jr., Leukotrienes, N. Engl. J. Med. 357 (18) (2007) 1841–1854, https://doi.org/10.1056/NEJMra071371.

[5] A. Koeberle, O. Werz, Inhibitors of the microsomal prostaglandin E(2) synthase-1 as alternative to non steroidal anti-inflammatory drugs (NSAIDs)–a critical review, Curr. Med. Chem. 16 (32) (2009) 4274–4296, https://doi.org/10.2174/092986709789578178.

[6] M. Iranshahi, M.G. Chini, M. Masullo, A. Sahebkar, A. Javidnia, M. Chitsazian Yazdi, C. Pergola, A. Koeberle, O. Werz, C. Pizza, S. Terracciano, S. Piacente, G. Bifulco, Can Small Chemical Modifications of Natural Pan-inhibitors Modulate the Biological Selectivity? The Case of Curcumin Prenylated Derivatives Acting as HDAC or mPGES-1 Inhibitors, J. Nat. Prod. 78 (12) (2015) 2867–2879, https://doi.org/10.1021/acs.jnatprod.5b00700.

[7] A. Minassi, G. Sánchez-Duffhues, J.A. Collado, E. Muñoz, G. Appendino, Dissecting the Pharmacophore of Curcumin. Which Structural Element Is Critical for Which Action? J. Nat. Prod. 76 (6) (2013) 1105–1112, https://doi.org/10.1021/np400148e.

[8] A. Caldarelli, E. Penucchini, D. Caprioglio, A.A. Genazzani, A. Minassi, Synthesis and tubulin-binding properties of non-symmetrical click C5-curcuminoids, Bioorg. Med. Chem. 21 (17) (2013) 5510–5517, https://doi.org/10.1016/j.bmc.2013.05.053.

[9] A. Koeberle, E. Muñoz, G.B. Appendino, A. Minassi, S. Pace, A. Rossi, C. Weinigel, D. Barz, L. Sautebin, D. Caprioglio, J.A. Collado, O. Werz, SAR Studies on Curcumin’s Pro-inflammatory Targets: Discovery of Prenylated Pyrazolocurcuminoids as Potent and Selective Novel Inhibitors of 5-Lipoxygenase, J. Med. Chem. 57 (13) (2014) 5638–5648, https://doi.org/10.1021/jm500308c.

[10] D. Caprioglio, S. Torretta, M. Ferrari, C. Travelli, A.A. Grolla, F. Condorelli, A. A. Genazzani, A. Minassi, Triazole-curcuminoids: A new class of derivatives for ‘tuning’ curcumin bioactivities? Bioorg. Med. Chem. 24 (2) (2016) 140–152, https://doi.org/10.1016/j.bmc.2015.11.044.

[11] H.P. Ammon, M.A. Wahl, Pharmacology of Curcuma longa, Planta Med. 57 (1) (1991) 1–7, https://doi.org/10.1055/s-2006-960004.

[12] T. Esatbeyoglu, P. Huebbe, I.M. Ernst, D. Chin, A.E. Wagner, G. Rimbach, Curcumin–from molecule to biological function, Angew. Chem. Int. Ed. 51 (22) (2012) 5308–5332, https://doi.org/10.1002/anie.201107724.

[13] P. Anand, A.B. Kunnumakkara, R.A. Newman, B.B. Aggarwal, Bioavailability of Curcumin: Problems and Promises, Mol. Pharm. 4 (6) (2007) 807–818, https://doi.org/10.1021/mp700113r.

[14] J. Barry, M. Fritz, J.R. Brender, P.E. Smith, D.K. Lee, A. Ramamoorthy, Determining the effects of lipophilic drugs on membrane structure by solid-state NMR spectroscopy: the case of the antioxidant curcumin, J. Am. Chem. Soc. 131 (12) (2009) 4490–4498, https://doi.org/10.1021/ja809217u.

[15] Y. Jiao, J. Wilkinson, E. Christine Pietsch, J.L. Buss, W. Wang, R. Planalp, F. M. Torti, S.V. Torti, Iron chelation in the biological activity of curcumin, Free Radical Biology and Medicine 40 (7) (2006) 1152–1160, https://doi.org/10.1016/j.freeradbiomed.2005.11.003.

[16] S. Awasthi, U. Pandya, S.S. Singhal, J.T. Lin, V. Thiviyanathan, W.E. Seifert, Y. C. Awasthi, G.A.S. Ansari, Curcumin-glutathione interactions and the role of human glutathione S-transferase P1–1, Chem. Biol. Interact. 128 (1) (2000) 19–38, https://doi.org/10.1016/s0009-2797(00)00185-x.

[17] Y. Jung, W. Xu, H. Kim, N. Ha, L. Neckers, Curcumin-induced degradation of ErbB2: A role for the E3 ubiquitin ligase CHIP and the Michael reaction acceptor activity of curcumin, Biochim. Biophys. Acta 1773 (3) (2007) 383–390, https://doi.org/10.1016/j.bbamcr.2006.11.004.

[18] E. Balogun, M. Hoque, P. Gong, E. Killeen, C.J. Green, R. Foresti, et al., Curcumin activates the haem oxygenase-1 gene via regulation of Nrf2 and the antioxidant-responsive element, Biochem. J. 371 (Pt 3) (2003) 887–895, https://doi.org/10.1042/bj20021619.

[19] S. Singh, B.B. Aggarwal, Activation of transcription factor NF-kappa B is suppressed by curcumin (diferuloylmethane) [corrected], J. Biol. Chem. 270 (42) (1995) 24995–25000, https://doi.org/10.1074/jbc.270.42.24995.

[20] N. Handler, W. Jaeger, H. Puschacher, K. Leisser, T. Erker, Synthesis of novel curcumin analogues and their evaluation as selective cyclooxygenase-1 (COX-1) inhibitors, Chem. Pharm. Bull. (Tokyo) 55 (1) (2007) 64–71, https://doi.org/10.1248/cpb.55.64.

[21] J. Hong, M. Bose, J. Ju, J.H. Ryu, X. Chen, S. Sang, et al., Modulation of arachidonic acid metabolism by curcumin and related beta-diketone derivatives: effects on cytosolic phospholipase A(2), cyclooxygenases and 5-lipoxygenase, Carcinogenesis 25 (9) (2004) 1671–1679, https://doi.org/10.1093/carcin/bgh165.

[22] C. Natarajan, J.J. Bright, Curcumin inhibits experimental allergic encephalomyelitis by blocking IL-12 signaling through Janus kinase-STAT pathway in T lymphocytes, J. Immunol. 168 (12) (2002) 6506–6513, https://doi.org/10.4049/jimmunol.168.12.6506.

[23] D.K. Agrawal, P.K. Mishra, Curcumin and its analogues: potential anticancer agents, Med. Res. Rev. 30 (5) (2010) 818–860, https://doi.org/10.1002/med.20188.

[24] R.A. Sharma, S.A. Euden, S.L. Platton, D.N. Cooke, A. Shafayat, H.R. Hewitt, et al., Phase I clinical trial of oral curcumin: biomarkers of systemic activity and compliance, Clin. Cancer Res. 10 (20) (2004) 6847–6854, https://doi.org/10.1158/1078-0432.Ccr-04-0744.

[25] A. Koeberle, H. Northoff, O. Werz, Curcumin blocks prostaglandin E2 biosynthesis through direct inhibition of the microsomal prostaglandin E2 synthase-1, Mol. Cancer Ther. 8 (8) (2009) 2348–2355, https://doi.org/10.1158/1535-7163.Mct-09-0290.

[26] C.A. Slabber, C.D. Grimmer, R.S. Robinson, Solution Conformations of Curcumin in DMSO, J. Nat. Prod. 79 (10) (2016) 2726–2730, https://doi.org/10.1021/acs.jnatprod.6b00726.

[27] S.P. Parimita, Y.V. Ramshankar, S. Suresh, T.N. Guru Row, Redetermination of curcumin: (1E,4Z,6E)-5-hydroxy-1,7-bis(4-hydroxy-3-methoxyphenyl)hepta-1,4,6-trien-3-one, Acta Crystallogr. E 63(2) (2007) o860-o862. DOI: doi:10.1107/S160053680700222X.

[28] A.M. Katsori, M. Chatzopoulou, K. Dimas, C. Kontogiorgis, A. Patsilinakos, T. Trangas, et al., Curcumin analogues as possible anti-proliferative & anti-inflammatory agents, Eur. J. Med. Chem. 46 (7) (2011) 2722–2735, https://doi.org/10.1016/j.ejmech.2011.03.060.

[29] R.I. Al-Wabli, T.M.M.H. Sakr, M.A. Khedr, A.A. Selim, M.A.E.-M.A. El-Rahman, W. A. Zaghary, Platelet-12 lipoxygenase targeting via a newly synthesized curcumin derivative radiolabeled with technetium-99m, Chem. Cent. J. 10 (2016) 73, https://doi.org/10.1186/s13065-016-0220-x.

[30] H. Ohtsu, Z. Xiao, J. Ishida, M. Nagai, H.-K. Wang, H. Itokawa, et al., Antitumor Agents. 217 .Curcumin Analogues as Novel Androgen Receptor Antagonists with Potential as Anti-Prostate Cancer Agents, J. Med. Chem. 45 (23) (2002) 5037–5042, https://doi.org/10.1021/jm020200g.

[31] T.T. Van Anh, A. Mostafa, Z. Rao, S. Pace, S. Schwaiger, C. Kretzer, et al., From Vietnamese plants to a biflavonoid that relieves inflammation by triggering the lipid mediator class switch to resolution, Acta Pharm. Sin. B 11 (6) (2021) 1629–1647, https://doi.org/10.1016/j.apsb.2021.04.011.

[32] A. Koeberle, U. Siemoneit, U. Buhring, H. Northoff, S. Laufer, W. Albrecht, et al., Licofelone suppresses prostaglandin E2 formation by interference with the inducible microsomal prostaglandin E2 synthase-1, J. Pharmacol. Exp. Ther. 326 (3) (2008) 975–982, https://doi.org/10.1124/jpet.108.139444.

[33] J.D. Ho, M.R. Lee, C.T. Rauch, K. Aznavour, J.S. Park, J.G. Luz, et al., Structure-based, multi-targeted drug discovery approach to eicosanoid inhibition: Dual inhibitors of mPGES-1 and 5-lipoxygenase activating protein (FLAP), Biochim. Biophys. Acta Mol. Gen. Subj. 1865 (2) (2021), 129800, https://doi.org/10.1016/j.bbagen.2020.129800.

[34] H. Pein, A. Ville, S. Pace, V. Temml, U. Garscha, M. Raasch, et al., Endogenous metabolites of vitamin E limit inflammation by targeting 5-lipoxygenase, Nat. Commun. 9 (1) (2018) 3834, https://doi.org/10.1038/s41467-018-06158-5.

[35] Z. Rao, S. Pace, P.M. Jordan, R. Bilancia, F. Troisi, F. Borner, et al., Vacuolar (H(+))-ATPase Critically Regulates Specialized Proresolving Mediator Pathways in Human M2-like Monocyte-Derived Macrophages and Has a Crucial Role in Resolution of Inflammation, J. Immunol. 203 (4) (2019) 1031–1043, https://doi.org/10.4049/jimmunol.1900236.

[36] P.M. Jordan, J. Gerstmeier, S. Pace, R. Bilancia, Z. Rao, F. Börner, et al., Staphylococcus aureus-Derived α-Hemolysin Evokes Generation of Specialized Pro-resolving Mediators Promoting Inflammation Resolution, Cell Rep. 33 (2) (2020), 108247, https://doi.org/10.1016/j.celrep.2020.108247.

[37] K. Neukirch, K. Alsabil, C.P. Dinh, R. Bilancia, M. Raasch, A. Ville, et al., Exploration of Long-Chain Vitamin E Metabolites for the Discovery of a Highly Potent, Orally Effective, and Metabolically Stable 5-LOX Inhibitor that Limits Inflammation, J. Med. Chem. 64 (15) (2021) 11496–11526, https://doi.org/10.1021/acs.jmedchem.1c00806.

[38] O. Werz, J. Gerstmeier, S. Libreros, X. De la Rosa, M. Werner, P.C. Norris, et al., Human macrophages differentially produce specific resolvin or leukotriene signals that depend on bacterial pathogenicity, Nat. Commun. 9 (1) (2018) 59, https://doi.org/10.1038/s41467-017-02538-5.

[39] D. Del Prete, E. Millán, F. Pollastro, G. Chianese, P. Luciano, J.A. Collado, et al., Turmeric Sesquiterpenoids: Expeditious Resolution, Comparative Bioactivity, and a New Bicyclic Turmeronoid, J. Nat. Prod. 79 (2) (2016) 267–273, https://doi.org/10.1021/acs.jnatprod.5b00637.

[40] S. Berger, D. Sicker, Classics in spectroscopy: isolation and structure elucidation of natural products, Chapter 3: Dyestuffs and Coloured Compounds, John Wiley & Sons, 2009.

[41] H.J.J. Pabon, A synthesis of curcumin and related compounds, Rec. Trav. Chim. Pays Bas 83 (4) (1964) 379–386, https://doi.org/10.1002/recl.19640830407.

[42] H.J. Koo, S. Shin, J.Y. Choi, K.H. Lee, B.T. Kim, Y.S. Choe, Introduction of Methyl Groups at C2 and C6 Positions Enhances the Antiangiogenesis Activity of Curcumin, Sci. Rep. 5 (2015) 14205, https://doi.org/10.1038/srep14205.

[43] S.K. Sandur, M.K. Pandey, B. Sung, K.S. Ahn, A. Murakami, G. Sethi, et al., Curcumin, demethoxycurcumin, bisdemethoxycurcumin, tetrahydrocurcumin and turmerones differentially regulate anti-inflammatory and anti-proliferative responses through a ROS-independent mechanism, Carcinogenesis 28 (8) (2007) 1765–1773, https://doi.org/10.1093/carcin/bgm123.

[44] H. Pei, Y. Yang, L. Cui, J. Yang, X. Li, Y. Yang, et al., Bisdemethoxycurcumin inhibits ovarian cancer via reducing oxidative stress mediated MMPs expressions, Sci. Rep. 6 (2016) 28773, https://doi.org/10.1038/srep28773.

[45] F. Jin, X. Chen, H. Yan, Z. Xu, B. Yang, P. Luo, et al., Bisdemethoxycurcumin attenuates cisplatin-induced renal injury through anti-apoptosis, anti-oxidant and anti-inflammatory, Eur. J. Pharmacol. 874 (2020), 173026, https://doi.org/10.1016/j.ejphar.2020.173026.

[46] H. Yang, Z. Du, W. Wang, M. Song, K. Sanidad, E. Sukamtoh, et al., Structure-Activity Relationship of Curcumin: Role of the Methoxy Group in Anti-inflammatory and Anticolitis Effects of Curcumin, J. Agric. Food Chem. 65 (22) (2017) 4509–4515, https://doi.org/10.1021/acs.jafc.7b01792.

[47] N.C. Gilbert, J. Gerstmeier, E.E. Schexnaydre, F. Börner, U. Garscha, D.B. Neau, et al., Structural and mechanistic insights into 5-lipoxygenase inhibition by natural products, Nat. Chem. Biol. 16 (7) (2020) 783–790, https://doi.org/10.1038/s41589-020-0544-7.

[48] S. Pace, K. Zhang, P.M. Jordan, R. Bilancia, W. Wang, F. Börner, et al., Anti-inflammatory celastrol promotes a switch from leukotriene biosynthesis to formation of specialized pro-resolving lipid mediators, Pharmacol. Res. 167 (2021), 105556, https://doi.org/10.1016/j.phrs.2021.105556.

[49] E. Israel, J. Cohn, L. Dubé, J.M. Drazen, P. Ratner, W. Pleskow, et al., Effect of Treatment With Zileuton, a 5-Lipoxygenase Inhibitor, Patients With Asthma: A Randomized Controlled Trial, JAMA 275 (12) (1996) 931–936, https://doi.org/10.1001/jama.1996.03530360041036.

[50] C.N. Serhan, N. Chiang, J. Dalli, B.D. Levy, Lipid mediators in the resolution of inflammation, Cold Spring Harb. Perspect. Biol. 7 (2) (2014), a016311, https://doi.org/10.1101/cshperspect.a016311.

[51] M. Bennett, D.W. Gilroy, Lipid Mediators in Inflammation, Microbiol. Spectr. 4(6) (2016). DOI: doi:10.1128/microbiolspec.MCHD-0035-2016.

[52] H.P. Ammon, H. Safayhi, T. Mack, J. Sabieraj, Mechanism of antiinflammatory actions of curcumine and boswellic acids, J. Ethnopharmacol. 38 (2–3) (1993) 113–119, https://doi.org/10.1016/0378-8741(93)90005-p.

[53] C.V. Rao, A. Rivenson, B. Simi, B.S. Reddy, Chemoprevention of colon carcinogenesis by dietary curcumin, a naturally occurring plant phenolic compound, Cancer Res. 55 (2) (1995) 259–266.

[54] J. Jankun, A.M. Aleem, S. Malgorzewicz, M. Szkudlarek, M.I. Zavodszky, D. L. Dewitt, et al., Synthetic curcuminoids modulate the arachidonic acid metabolism of human platelet 12-lipoxygenase and reduce sprout formation of human endothelial cells, Mol. Cancer Ther. 5 (5) (2006) 1371–1382, https://doi.org/10.1158/1535-7163.Mct-06-0021.

[55] K.M. Nelson, J.L. Dahlin, J. Bisson, J. Graham, G.F. Pauli, M.A. Walters, The Essential Medicinal Chemistry of Curcumin, J. Med. Chem. 60 (5) (2017) 1620–1637, https://doi.org/10.1021/acs.jmedchem.6b00975.

[56] J.F. Costello, L.S. Dunlop, P.J. Gardiner, Characteristics of prostaglandin induced cough in man, Br J Clin Pharmacol 20 (4) (1985) 355–359, https://doi.org/10.1111/j.1365-2125.1985.tb05077.x.

[57] E. Melillo, K.L. Woolley, P.J. Manning, R.M. Watson, P.M. O'Byrne, Effect of inhaled PGE2 on exercise-induced bronchoconstriction in asthmatic subjects, Am. J. Respir. Crit. Care Med. 149 (5) (1994) 1138–1141, https://doi.org/10.1164/ajrccm.149.5.8173753.

[58] L. Arshad, M.A. Haque, S.N.A. Bukhari, I. Jantan, An overview of structure–activity relationship studies of curcumin analogs as antioxidant and anti-inflammatory agents, Future Med. Chem. 9 (6) (2017) 605–626, https://doi.org/10.4155/fmc-2016-0223.

[59] M.R. Peram, S.S. Jalalpure, M.B. Palkar, P.V. Diwan, Stability studies of pure and mixture form of curcuminoids by reverse phase-HPLC method under various experimental stress conditions, Food Sci Biotechnol 26 (3) (2017) 591–602, https://doi.org/10.1007/s10068-017-0087-1.

[60] G. Appendino, P. Allegrini, E. de Combarieu, F. Novicelli, G. Ramaschi, N. Sardone, Shedding light on curcumin stability, Fitoterapia 156 (2022), 105084, https://doi.org/10.1016/j.fitote.2021.105084.

[61] H. Ahsan, N. Parveen, N.U. Khan, S.M. Hadi, Pro-oxidant, anti-oxidant and cleavage activities on DNA of curcumin and its derivatives demethoxycurcumin and bisdemethoxycurcumin, Chem. Biol. Interact. 121 (2) (1999) 161–175, https://doi.org/10.1016/s0009-2797(99)00096-4.

[62] L.Y. Guo, X.F. Cai, J.J. Lee, S.S. Kang, E.M. Shin, H.Y. Zhou, et al., Comparison of suppressive effects of demethoxycurcumin and bisdemethoxycurcumin on expressions of inflammatory mediators in vitro and in vivo, Arch. Pharm. Res. 31 (4) (2008) 490–496, https://doi.org/10.1007/s12272-001-1183-8.

[63] K. Gouthamchandra, H.V. Sudeep, S. Chandrappa, A. Raj, P. Naveen, K. Shyamaprasad, Efficacy of a Standardized Turmeric Extract Comprised of 70% Bisdemothoxy-Curcumin (REVERC3) Against LPS-Induced Inflammation in RAW264.7 Cells and Carrageenan-Induced Paw Edema, J. Inflamm. Res. 14 (2021) 859–868, https://doi.org/10.2147/jir.S291293.

[64] A.I. Joseph, R.L. Edwards, P.B. Luis, S.H. Presley, N.A. Porter, C. Schneider, Stability and anti-inflammatory activity of the reduction-resistant curcumin analog, 2,6-dimethyl-curcumin, Org. Biomol. Chem. 16 (17) (2018) 3273–3281, https://doi.org/10.1039/c8ob00639c.

[65] W. Ahmad, E. Kumolosasi, I. Jantan, S.N.A. Bukhari, M. Jasamai, Effects of Novel Diarylpentanoid Analogues of Curcumin on Secretory Phospholipase A2, Cyclooxygenases, Lipo-oxygenase, and Microsomal Prostaglandin E Synthase-1, Chem. Biol. Drug Des. 83 (6) (2014) 670–681, https://doi.org/10.1111/cbdd.12280.

[66] K.-H. Lee, F.H. Ab. Aziz, A. Syahida, F. Abas, K. Shaari, D.A. Israf, et al., Synthesis and biological evaluation of curcumin-like diarylpentanoid analogues for anti-inflammatory, antioxidant and anti-tyrosinase activities, Eur. J. Med. Chem. 44(8) (2009) 3195-3200. DOI: 10.1016/j.ejmech.2009.03.020.

[67] E. Skrzypczak-Jankun, N.P. McCabe, S.H. Selman, J. Jankun, Curcumin inhibits lipoxygenase by binding to its central cavity: theoretical and X-ray evidence, Int. J. Mol. Med. 6 (5) (2000) 521–526, https://doi.org/10.3892/ijmm.6.5.521.

[68] E. Skrzypczak-Jankun, K. Zhou, N.P. McCabe, S.H. Selman, J. Jankun, Structure of curcumin in complex with lipoxygenase and its significance in cancer, Int. J. Mol. Med. 12 (1) (2003) 17–24, https://doi.org/10.3892/ijmm.12.1.17.

[69] E. Chainoglou, A. Siskos, E. Pontiki, D. Hadjipavlou-Litina, Hybridization of Curcumin Analogues with Cinnamic Acid Derivatives as Multi-Target Agents Against Alzheimer's Disease Targets, Molecules (Basel, Switzerland) 25 (21) (2020) 4958, https://doi.org/10.3390/molecules25214958.

[70] S.N.A. Bukhari, G. Lauro, I. Jantan, G. Bifulco, M.W. Amjad, Pharmacological evaluation and docking studies of α, β-unsaturated carbonyl based synthetic compounds as inhibitors of secretory phospholipase A2, cyclooxygenases, lipoxygenase and proinflammatory cytokines, Bioorg. Med. Chem. 22 (15) (2014) 4151–4161, https://doi.org/10.1016/j.bmc.2014.05.052.

[71] M.E. Newcomer, A.R. Brash, The structural basis for specificity in lipoxygenase catalysis, Protein Sci 24 (3) (2015) 298–309, https://doi.org/10.1002/pro.2626.

[72] N.C. Gilbert, S.G. Bartlett, M.T. Waight, D.B. Neau, W.E. Boeglin, A.R. Brash, et al., The structure of human 5-lipoxygenase, Science 331 (6014) (2011) 217–219, https://doi.org/10.1126/science.1197203.

[73] C.N. Serhan, Pro-resolving lipid mediators are leads for resolution physiology, Nature 510 (7503) (2014) 92–101, https://doi.org/10.1038/nature13479.

[74] C.N. Serhan, K. Gotlinger, S. Hong, Y. Lu, J. Siegelman, T. Baer, et al., Anti-inflammatory actions of neuroprotectin D1/protectin D1 and its natural stereoisomers: assignments of dihydroxy-containing docosatrienes, J. Immunol. 176 (3) (2006) 1848–1859, https://doi.org/10.4049/jimmunol.176.3.1848.

[75] N.H. Schebb, H. Kühn, A.S. Kahnt, K.M. Rund, V.B. O'Donnell, N. Flamand, et al., Formation, Signaling and Occurrence of Specialized Pro-Resolving Lipid Mediators-What is the Evidence so far? Front. Pharmacol. 13 (2022), 838782 https://doi.org/10.3389/fphar.2022.838782.

[76] S. Chen, H. Liang, Y. Ji, H. Kou, C. Zhang, G. Shang, et al., Curcumin Modulates the Crosstalk Between Macrophages and Bone Mesenchymal Stem Cells to Ameliorate Osteogenesis, Front. Cell Dev. Biol. 9 (2021), 634650, https://doi.org/10.3389/fcell.2021.634650.

[77] C. Kretzer, P.M. Jordan, R. Bilancia, A. Rossi, T. Gür Maz, E. Banoglu, et al., Shifting the Biosynthesis of Leukotrienes Toward Specialized Pro-Resolving Mediators by the 5-Lipoxygenase-Activating Protein (FLAP) Antagonist BRP-201, J. Inflamm. Res. 15 (2022) 911–925, https://doi.org/10.2147/jir.S345510.

[78] B.D. Levy, C.B. Clish, B. Schmidt, K. Gronert, C.N. Serhan, Lipid mediator class switching during acute inflammation: signals in resolution, Nat. Immunol. 2 (7) (2001) 612–619, https://doi.org/10.1038/89759.